Journal of Advanced Research 60 (2024) 141–157

Contents lists available at ScienceDirect

Journal of Advanced Research

journal homepage: www.elsevier.com/locate/jare

Original Article

Inhibition of oxidative stress-induced epithelial-mesenchymal transition in retinal pigment epithelial cells of age-related macular degeneration model by suppressing ERK activation

Ya-Chi Yang [a,b], Yueh Chien [a,b,1], Aliaksandr A. Yarmishyn [a,b,1], Lee-Yieng Lim [a,1], Hao-Yu Tsai [a,c], Wen-Chuan Kuo [d], Ping-Hsing Tsai [a,b,c], Sheng-Hsien Yang [d], Shao-I Hong [a,c], Shih-Jen Chen [b,e], De-Kuang Hwang [b,e], Yi-Ping Yang [a,b,c,*], Shih-Hwa Chiou [a,b,c,e,f,*]

[a] Department of Medical Research, Taipei Veterans General Hospital, Taipei 112201, Taiwan
[b] College of Medicine, National Yang Ming Chiao Tung University, Taipei 112304, Taiwan
[c] Institute of Pharmacology, College of Medicine, National Yang Ming Chiao Tung University, Taipei 112304, Taiwan
[d] Institute of Biophotonics, College of Biomedical Science and Engineering, National Yang Ming Chiao Tung University, Taipei 112304, Taiwan
[e] Department of Ophthalmology, Taipei Veterans General Hospital, Taipei 112201, Taiwan
[f] Genomic Research Center, Academia Sinica, Taipei 115024, Taiwan

HIGHLIGHTS

- $NaIO_3$ was demonstrated to induce EMT in human ARPE-19 cells and in RPE cells of the mouse eyes as an AMD model.
- Ca^{2+}, EGFR, and ERK signaling pathways responded to $NaIO_3$-induced EMT in ARPE-19 cells.
- Post-treatment with FR180204 downregulated multiple $NaIO_3$-induced signaling pathways leading to EMT.
- ERK was shown to play a critical role in promoting oxidative stress-induced EMT of ARPE-19 cells in contrast to MEK.
- FR180204 restored the RPE integrity and retinal morphology compromised by $NaIO_3$ in mouse retina.

GRAPHICAL ABSTRACT

Activation of ERK is critical for $NaIO_3$-induced multiple signaling pathways to coordinate EMT in RPE cells.

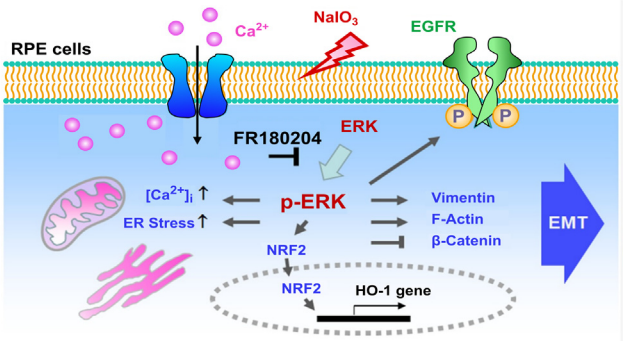

ARTICLE INFO

Article history:
Received 22 March 2023
Revised 5 May 2023
Accepted 11 June 2023
Available online 15 June 2023

ABSTRACT

Introduction: Epithelial-mesenchymal transition (EMT) of retinal pigment epithelial (RPE) cells is related to the pathogenesis of various retinopathies including age-related macular degeneration (AMD). Oxidative stress is the major factor that induces degeneration of RPE cells associated with the etiology of AMD.

Objectives: Sodium iodate ($NaIO_3$) generates intracellular reactive oxygen species (ROS) and is widely used to establish a model of AMD due to the selective induction of retinal degeneration. This study

Abbreviations: AMD, age-related macular degeneration; EMT, epithelial-mesenchymal transition; RPE cells, retinal pigment epithelial cells; ROS, reactive oxygen species; SD-OCT, spectral domain optical coherence tomography; EGFR, epidermal growth factor receptor; ERK, extracellular signal-regulated kinase; p-EGFR, phospho-EGFR; p-ERK, phospho-ERK; ER, endoplasmic reticulum; RSKs, p90 ribosomal S6 kinases; CCK-8, Cell Counting Kit-8; LDH, lactate dehydrogenase; HRF, hyperreflective retinal foci.

* Corresponding authors at: Department of Medical Research, Taipei Veterans General Hospital, No. 201, Sec. 2 Shipai Rd. Beitou Dist., Taipei 112201, Taiwan.
E-mail addresses: molly0103@gmail.com (Y.-P. Yang), shchiou@vghtpe.gov.tw (S.-H. Chiou).

[1] Yueh Chien, Aliaksandr A. Yarmishyn, and Lee-Yieng Lim contibuted equally to this work.

https://doi.org/10.1016/j.jare.2023.06.004

Keywords:
Retinopathy
Extracellular signal-regulated kinase
Epithelial growth factor receptor
Calcium signaling
Reactive oxygen species
FR180204

was performed to clarify the effects of multiple $NaIO_3$-stimulated signaling pathways on EMT in RPE cells.
Methods: The EMT characteristics in $NaIO_3$-treated human ARPE-19 cells and RPE cells of the mouse eyes were analyzed. Multiple oxidative stress-induced modulators were investigated and the effects of pre-treatment with Ca^{2+} chelator, extracellular signal-related kinase (ERK) inhibitor, or epidermal growth factor receptor (EGFR) inhibitor on $NaIO_3$-induced EMT were determined. The efficacy of post-treatment with ERK inhibitor on the regulation of $NaIO_3$-induced signaling pathways was dissected and its role in retinal thickness and morphology was evaluated by using histological cross-sections and spectral domain optical coherence tomography.
Results: We found that $NaIO_3$ induced EMT in ARPE-19 cells and in RPE cells of the mouse eyes. The intracellular ROS, Ca^{2+}, endoplasmic reticulum (ER) stress marker, phospho-ERK, and phospho-EGFR were increased in $NaIO_3$-stimulated cells. Our results showed that pre-treatment with Ca^{2+} chelator, ERK inhibitor, or EGFR inhibitor decreased $NaIO_3$-induced EMT, interestingly, the inhibition of ERK displayed the most prominent effect. Furthermore, post-treatment with FR180204, a specific ERK inhibitor, reduced intracellular ROS and Ca^{2+} levels, downregulated phospho-EGFR and ER stress marker, attenuated EMT of RPE cells, and prevented structural disorder of the retina induced by $NaIO_3$.
Conclusions: ERK is a crucial regulator of multiple $NaIO_3$-induced signaling pathways that coordinate EMT program in RPE cells. Inhibition of ERK may be a potential therapeutic strategy for the treatment of AMD.

Introduction

Age-related macular degeneration (AMD) is a retinal degenerative disease, which is the principal cause of blindness among people over 65 years old in developed countries [1]. The pathogenesis of AMD is related to the degradation of retinal pigment epithelial (RPE) cells and affects macula region of the retina, resulting in central vision impairment upon its progression [2]. Besides age and genetic background, oxidative stress is one of the most important etiological factors in AMD. Indeed, RPE cells are subjected to particularly high oxidative stress environment due to specific physiological reactive oxygen species (ROS) sources such as high metabolic activity to support the retina [3] and phagocytosis to digest photoreceptor outer segments [4]. Importantly, the degenerative RPE cells are exposed to more abundant accumulation of ROS associated with the decreased capacity to neutralize ROS and the diminished autophagy ability related to aging [5].

Epithelial-mesenchymal transition (EMT) is a biological process of epithelial cells undergoing a transformation into mesenchymal cells [6]. EMT is classified into three different subtypes associated with distinct biological processes. The type I EMT is associated with implantation and organ development and the type III occurs in neoplastic cells, the type II EMT is associated with the wound healing and tissue regeneration and is induced by trauma and inflammatory injury to reconstruct tissues [7]. Previous animal and cell culture studies support the idea that RPE cells undergo type II EMT to move along a continuum from epithelial cells toward mesenchymal cells [6]. Type II EMT is associated with RPE cell dysfunction resultant from aging, inflammation, or impaired tight junctions [8]. Such dysfunctional RPE cells become less differentiated and subsequently undergo EMT [9] and have been found in various retinal diseases including AMD [6], inherited macular degenerations [8], retinitis pigmentosa [10,11], and proliferative vitreoretinopathy [12,13]. The consequences of such events may lead to the migration of RPE cells into the neuroretina in macular degeneration and into the epiretinal area in proliferative vitreoretinopathy [8].

$NaIO_3$ can elicit ROS production, including hydrogen peroxide (H_2O_2) and superoxide anions ($O_2^{\bullet-}$), to enhance oxidative stress response in ARPE-19 cells [14]. As a result, the dysfunctional RPE layer appears to disintegrate and initiate translocation after the *retro*-orbital $NaIO_3$ injection in mice [15]. Among the components of oxidative stress response program induced by $NaIO_3$-derived ROS were superoxide dismutase [16,17], glutathione peroxidase [17], caspase 3 [18], and 8-isoprostane [17], as was shown in ARPE-19 cells or in the rat retina. $NaIO_3$ administration has been widely used as a dry AMD model for its reproducible and selective induction of retinal degeneration [19–21]. However, the potential mechanism of $NaIO_3$-induced oxidative stress in EMT of RPE cells is still unclarified [22]. Several molecular modulators have been revealed to regulate EMT in cells, including Ca^{2+} signaling, extracellular signal-related kinase (ERK), and epidermal growth factor receptor (EGFR). Briefly, the attenuation of Ca^{2+} signaling by intracellular Ca^{2+} chelation significantly reduced EGF-induced EMT [23], and the activation of EGFR [24] and ERK [25] was required for TGF-β1-induced EMT in cancer cells. Nevertheless, the roles of Ca^{2+}, phospho-ERK (p-ERK), and phospho-EGFR (p-EGFR) in the mechanism regulating $NaIO_3$-induced EMT in RPE cells have not been characterized.

Anti-vascular endothelial growth factor (anti-VEGF) drugs are the most effective therapy for the wet-type AMD [26,27], however, there are currently no valid treatments for the most common dry-type AMD [28]. Therefore, the development of potential therapeutic agents for the treatment of dry AMD is necessary. Moreover, oxidative stress is known as an important factor to induce AMD, and EMT of RPE cells is implicated in the pathogenesis of various retinopathies including AMD [8–13]. However, the mechanism involved in oxidative stress-induced EMT in RPE cells is not clarified. In this study, we aimed to investigate the effect of the ROS on multiple pathways that coordinate EMT in RPE cells. These results may provide new insights into the intracellular pathways responsible for regulating oxidative stress-induced EMT in RPE cells in the progression of AMD.

Methods

Cell culture and chemicals

We purchased human ARPE-19 (#CRL-2302) from ATCC and maintained the cells in culture medium which included Dulbecco's modified Eagle's medium (DMEM)/F-12 (#11330–032), 10% fetal bovine serum, and penicillin/streptomycin (#15140–122), all purchased from Gibco/Thermo Fisher Scientific (Waltham, MA, USA). The cells were cultured at 37 °C under 5% CO_2 atmosphere with 95% relative humidity. The cells were seeded at a density of

3 $\times 10^5$ cells/ml at day 1. After reaching 80–90% of confluence at day 3, the cells were starved and synchronized in serum-free DMEM/F-12 for 24 h before being subjected to further treatment with $NaIO_3$ or inhibitors (**Fig. S1**). 500 nM BAPTA-AM [29], 50 nM erlotinib [30], 10 μM FR180204 [31,32], 2 μM U0126, and 1 to 4 μM BVD-523 were used in cell culture. $NaIO_3$ (#71702), H_2O_2 (#31642), BAPTA-AM (#A1076), erlotinib (#SML2156), and FR180204 (#SML0320) were purchased from Sigma-Aldrich (St. Louis, MO, USA). BVD-523 (ulixertinib, #S7854) was obtained from Selleck Chemicals (Houston, TX, USA). Fluo-4 AM (#F14201), CellROX Green (#C10444) and DHR123 (#D23806) were purchased from Thermo Fisher Scientific.

Western blot analysis

ARPE-19 cells were lysed in RIPA lysis buffer (#20–188; Merck Millipore, Burlington, MA, USA) containing protease inhibitor (#11836153001; Roche, Basel, Switzerland) and phosphatase inhibitor PhosSTOP (#04906837001; Roche, Basel, Switzerland). The samples were centrifuged for 10 min at 13,000 rpm and 4℃ to obtain the supernatant for analysis [33,34]. The protein concentrations were determined using the BCA Protein Assay Kit (#23225; Thermo Fisher Scientific). The information on the used antibodies is listed in **Supplementary Table 1**. The tagged secondary antibodies were detected by enhanced chemiluminescence (ECL) substrate kit (Merck Millipore, Darmstadt, Germany). The intensities of immunoblot bands were quantified using ImageJ software (U.S. National Institutes of Health, Bethesda, MD, USA).

Immunofluorescence and phalloidin staining

ARPE-19 cells were seeded at a density of 3×10^5 cells/ml on glass coverslips in 24-well plates and incubated in a 5% CO_2 incubator at 37 °C until the cells were approximately 80% confluent. After 1 day of incubation with serum-free medium, cells were treated with 1 to 2 mM $NaIO_3$ in HBSS for 24 h and then treated with various inhibitors (**Fig. S1**). The information on the used antibodies is listed in **Supplementary Table 1**. After the mounting procedure, images were captured with a 63x objective for ARPE-19 cells and 40x objective for whole mount mouse retinas using a confocal laser scanning microscope (LSM 880; ZEISS, Oberkochen, Germany) and ZEN software was used for image processing [33,35,36].

Ca^{2+} imaging and $[Ca^{2+}]i$ detection

After the respective treatments (**Fig. S1**), ARPE-19 cells were incubated with 5 μM Fluo-4 AM for 30 min in a 5% CO_2 incubator at 37 °C with 95% relative humidity, followed by washing with HBSS to remove the excess Fluo-4 AM. Then, the cells were incubated in HBSS without Ca^{2+} (#14175095; Thermo Fisher Scientific), and the fluorescence intensity of Fluo-4 AM was recorded for 180 s by a fluorescent microscope (Olympus IX71; Olympus Corporation, Tokyo, Japan) at 1 s intervals using a FITC filter. At 30 s after starting the recording, ARPE-19 cells were continuously exposed to 1 mM H_2O_2 to stimulate Ca^{2+} release from intracellular storage [37]. 5 μM BAPTA-AM, a non-fluorescent Ca^{2+} chelator, was applied to the cells for obtaining the minimal fluorescence (F_{min}) intensity of Fluo-4 AM in individual cells. ARPE-19 cells were incubated in Ca^{2+}-containing HBSS (#14025092; Thermo Fisher Scientific) and 5 μM A23187, Ca^{2+} ionophore, for the acquirement of the maximal fluorescence (F_{max}) intensity of Fluo-4 AM in individual cells. The following formula was used for Ca^{2+} calibration: $[Ca^{2+}]_i = K_d[F-F_{min}]/[F_{max}-F]$. The average fluorescence intensities in individual ARPE-19 cells were quantified using region of interest (ROI) analysis in ImageJ software.

ROS measurement

We monitored $NaIO_3$-induced ROS in live cells by two fluorescent sensors, CellROX Green [36] and DHR123 [38]. The cells were incubated with 5 μM CellROX or 10 μM DHR123 for 30 min in an incubator at 37 °C in 5% CO_2 with 95% relative humidity. The fluorescence intensity was estimated by a fluorescence microscope (Olympus IX71, Olympus Corporation) using a FITC filter. Average fluorescence intensities in individual ARPE-19 cells were quantified using region of interest (ROI) analysis with ImageJ software.

Wound healing assay

ARPE-19 cells were seeded in wells with Culture-Inserts (ibidi, Gräfelfing, Germany) and treated as per experimental design. After the Culture-Inserts were removed to reveal the wound gap, the cells were incubated with mitomycin (500 ng/ml) and $NaIO_3$ in serum-free medium for 24 h. To investigate the pre-treatment or post-treatment effects of small molecule inhibitors, the cells were administered with various inhibitors under conditions described in **Fig. S1**. The baseline and the wound closure after treatment were photographed at magnification of 200 × by a digital microscope (Olympus IX71; Olympus Corporation).

Cell viability and cytotoxicity assays

Cell Counting Kit-8 (CCK-8; Sigma-Aldrich) was used to quantitatively evaluate cell viability [39]. The ARPE-19 cells were seeded in 96-well plates at a density of 3 $\times$ 10^5 cells per ml and then treated with $NaIO_3$ (0, 1, 1.5, and 2 mM) as described in Fig. S1A. Then, 10 μL of CCK-8 solution was added to each well of the plate, which was then maintained for 2 h in a 5% CO_2 incubator at 37 °C. The level of lactate dehydrogenase (LDH) released from the cells was measured to determine $NaIO_3$-induced cellular toxicity using the CyQUANT LDH Cytotoxicity Assay (#C20301; Thermo Fisher Scientific) [40]. All samples were assayed in triplicate for CCK-8 and LDH content at a wavelength of 450 nm (CCK-8) and 490 nm (LDH) using a Sunrise microplate reader (Tecan, Männedorf, Switzerland).

ELISA measurement of BMP4, TGF-β1, and EGF secretion levels

Human BMP4 ELISA kit (#E-EL-H0012; Elabscience, Wuhan, China), human TGF-β1 Quantikine ELISA kit (#DB100B; R&D Systems, Minneapolis, MN, USA), and human EGF Quantikine ELISA kit (#DEG00; R&D Systems, Minneapolis, MN, USA) were used according to the manufacturer's instructions. The reactions were quantified by optical density measurement using a Sunrise automated ELISA reader (Tecan).

Mouse model of $NaIO_3$-induced oxidative stress in the retina

To investigate the effects of $NaIO_3$ on the retina *in vivo*, we conducted *retro*-orbital $NaIO_3$ injection in 8-week-old C57BL/6J mice as described in the previous studies [15,41]. Briefly, sterile 1% $NaIO_3$ solution was prepared freshly for injection via the *retro*-orbital sinus at 20 mg/kg body weight after mice were anesthetized. Control mice were injected with PBS in parallel. Intraperitoneal (IP) injection of $NaIO_3$ was performed as described previously [42]. To study the effect of FR180204 on $NaIO_3$-induced lesion of the retina and EMT of RPE cells, 100 nM FR180204 was *retro*-orbitally injected into the right eye and diluted DMSO was parallelly injected into the left eye as a control at 16 h after $NaIO_3$ IP or *retro*-orbital injection.

Histological analysis of the retina

The methodology for fixation, dehydration, infiltration, and embedding was applied according to the protocol (Bio-Check Laboratories, New Taipei City, Taiwan) [43]. Briefly, whole eyes were enucleated and fixed with 4% paraformaldehyde overnight, followed by three washes in PBS. After paraffin embedding, each sample was sectioned into 3 μm slices and stained with hematoxylin and eosin (H&E). The morphology of the retina was observed using a digital inverted microscope (Olympus IX71; Olympus Corporation).

Spectral domain ocular coherence tomography (SD-OCT)

The SD-OCT system has been established in our previous study [44]. In short, an illumination source used was SuperK Extreme supercontinuum fiber laser (NKT Photonics, Birkerød, Denmark) with broadband of which the wavelength range is 650–1800 nm. For our experimental measurements, we applied the center wavelength at 850 nm with full-width half maximum at 140 nm. To direct the light to the sample and reference arms of the interferometer, we used 20/80 fiber optic couplers. A spectrometer with a 2048 pixels line scan sensor and 130 kHz maximum A-line scan rate was used to record the interference signal. A total of 500 A-scans were used to generate one 2D image. System control and signal acquisition were achieved using LabView software. The en face images of the retina were obtained from B-scan data using a Z-projection method of the ImageJ software [45].

RNA-Seq analysis

Total RNA was prepared as described in our previous study [46]. For generation of strand-specific libraries, we used 500 ng of total RNA extracted by the TruSeq Stranded Total RNA Library Prep Kit (Illumina, San Diego, CA, USA). Then we used an Illumina HiSeq 2000 sequencer to perform pair-end sequencing (150 bp reads) of cDNA libraries. The alignment of the reads to the human genome (GRCh38/hg38) was accomplished with TopHat v1.3.3, and one alignment with up to two mismatches per read was allowed. For calculation of mRNA TPM values, we used the DRAGEN mRNA quantification pipeline (Illumina). For selection of the differentially expressed genes, we applied the criteria as follows: the minimum RPKM above 10 units, fold change more than 1.5-fold or less than 0.85-fold. Clustering heatmaps were generated using Orange software (https://orange.biolab.si). Principal component analysis (PCA) and bubble enrichment analysis were performed with the princomp and pathfindR R packages. The gene ontology (GO) analysis was performed with the Enrichr software (https://maayanlab.cloud/Enrichr/). The overlapped genes with log2 intensity were used to establishe a dataset to perform GSEA analysis (https://www.broadinstitute.org/gsea/).

Statistical analysis

All statistical analyses were performed using SPSS 17.0 statistical software. A two-tail Student's *t*-test was used for statistical comparison between two groups. One-way ANOVA and post hoc analysis with Scheffé test for multiple tests were used [47,48]. The experiment data are presented as the means ± standard errors of the means. $p < 0.05$ was taken as significant.

Results

$NaIO_3$-induced oxidative stress increases EMT capacity of RPE cells

Oxidative stress plays an important role in RPE cell degeneration during AMD [3]. Previous studies have found that $NaIO_3$ leads to ROS production and cell dysfunction in ARPE-19 cells [18] as well as the RPE cells of the mouse retina [15,19], which were used as *in vitro* and *in vivo* models for investigating pathogenic mechanism of AMD. As the initial step of our study, we aimed to validate the potential role of oxidative stress in the induction of EMT in RPE cells. Therefore, ARPE-19 cells were cultured in a serum starvation medium for 24 h in order to synchronize the cells and eliminate serum-induced activation of various signaling pathways such as Raf/MEK/ERK and PI3K/AKT pathways which may result in the interference with the observed drug effects. Afterwards, the cells were treated with $NaIO_3$ in a concentration range from 1 to 2 mM for 24 h (Fig. S1**A**). The concentrations of $NaIO_3$ of 1 and 1.5 mM did not have significant effect on the viability or cytotoxicity of ARPE-19 cells, and 2 mM $NaIO_3$ only very marginally reduced their viability or cytotoxicity (Fig. S2**A and B**). The expression of EMT markers was monitored by western blotting and it was revealed that the protein level of β-catenin (epithelial marker) decreased in $NaIO_3$ concentration-dependent manner, at the same time, the levels of vimentin and Snail (EMT markers) increased (Fig. 1**A and B**). Interestingly, the maximum expression level of vimentin was achieved at 2 mM $NaIO_3$; however, the highest expression of Snail occurred at 1.5 mM $NaIO_3$ (Fig. 1**A and B**). Fluorescent staining with phalloidin revealed the increased F-actin polymerization with the formation of the filopodia structures typical for the mesenchymal cell types (Fig. 1**C**). At the same time, immunofluorescent staining showed upregulation of vimentin and downregulation of β-catenin (Fig. 1**C**). Consistently with the fact that the transition to mesenchymal phenotype leads to the increased motility of cells, we observed that the treatment with $NaIO_3$ also resulted in the increased migration of ARPE-19 cells as was demonstrated by wound healing assay (Fig. 1**D**). To summarize, we confirmed that ARPE-19 cells treated with sublethal concentrations of $NaIO_3$ could be a usable *in vitro* model for oxidative stress-induced EMT. Moreover, to further confirm the effect of $NaIO_3$ on EMT induction *in vivo*, we performed *retro*-orbital injection of $NaIO_3$ into mouse eyes (Fig. 1**E**). Indeed, such injection resulted in significant detachment of the RPE cells and their upward migration into the outer segment layer of photoreceptors accompanied by clearly disorganized structures of inner and outer segments as well as outer nuclear layer (Fig. 1**F**). To summarize, $NaIO_3$ was shown to induce EMT in RPE cells both *in vitro* and *in vivo*.

Characterization of pathway responses to the $NaIO_3$-induced oxidative stress resulting in EMT of ARPE-19 cells

Next, we aimed to further dissect the pathways of the induction of EMT by the oxidative stress. Indeed, the treatment of ARPE-19 cells with $NaIO_3$ for 24 h induced the production of intracellular ROS in a concentration-dependent manner as was demonstrated by CellROX and DHR123 assays (Fig. 2**A and B**). There is multiple evidence pointing out that ROS and Ca^{2+} signaling have a cross-talk relationship, particularly in age-related diseases [49]; in addition, the EMT of cells has been known to occur in a Ca^{2+} signaling-dependent manner [23]. Therefore, we measured intracellular Ca^{2+} concentration ($[Ca^{2+}]_i$) in $NaIO_3$-stimulated ARPE-19 cells using Fluo-4 AM fluorescent Ca^{2+} indicator (Fig. 2**C and** Fig. S3**A**), and stimulated cells with H_2O_2 to release Ca^{2+} from the intracellular storage [37,50]. It was shown that the basal level of $[Ca^{2+}]_i$ increased (Fig. 2**D**), and Ca^{2+} in intracellular storage was elevated (Fig. 2**E**) after the treatment with $NaIO_3$. Normally, cells exposed to oxidative stress initiate a complex antioxidant response dependent on NRF2 transcription factor [51]. Indeed, the treatment of ARPE-19 with $NaIO_3$ for 24 h resulted in the increased NRF2 protein levels at 1 and 1.5 mM concentrations (Fig. 2**F**). At the same time, the protein level of heme oxygenase-1 (HO-1), which is a tar-

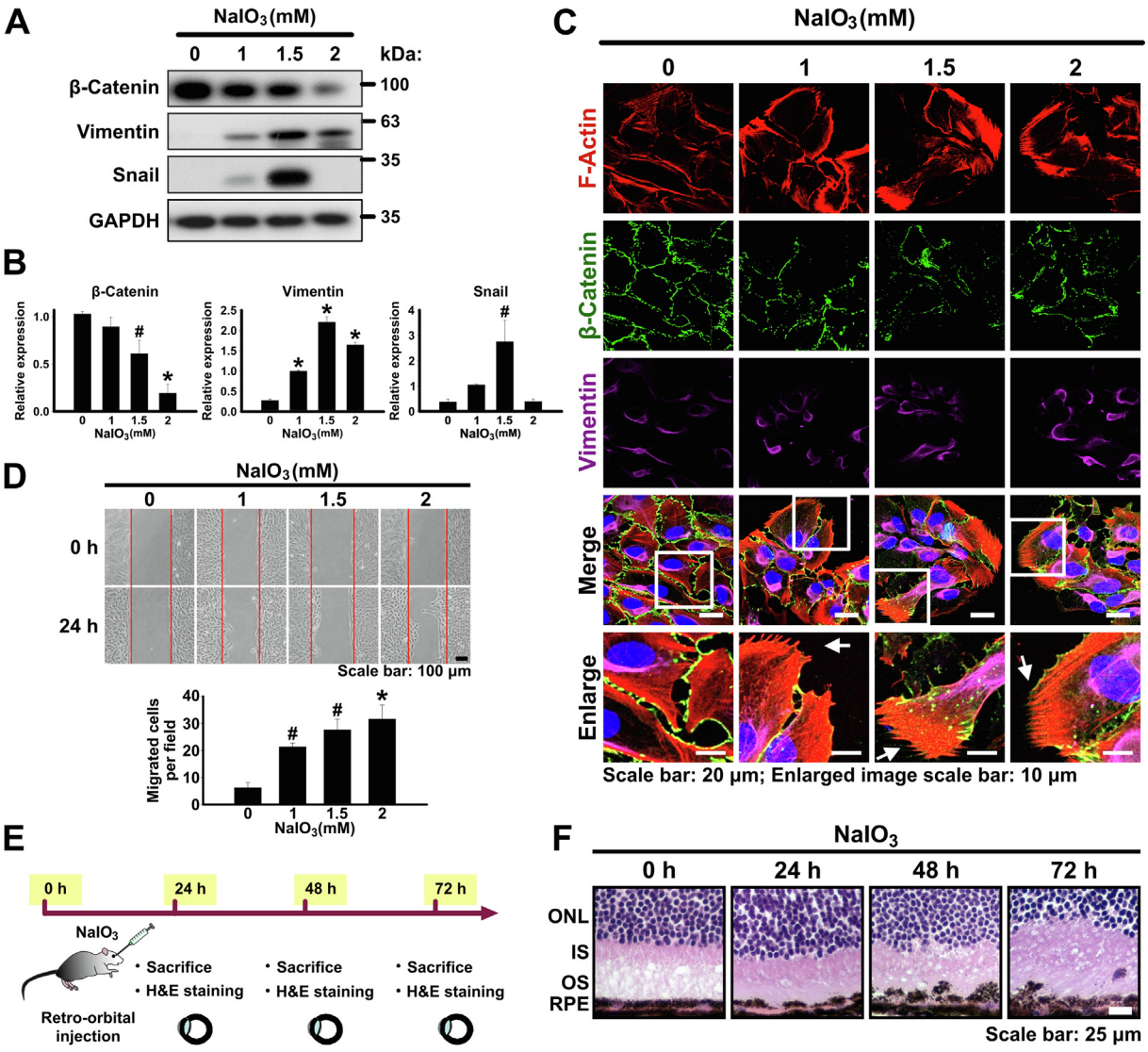

Fig. 1. $NaIO_3$-induced oxidative stress increases EMT capacity of RPE cells. (**A**) Immunoblotting analysis of the expression of the epithelial (β-catenin) and mesenchymal (Snail and vimentin) markers in ARPE-19 cells upon the treatment with the indicated concentrations of $NaIO_3$. GAPDH – loading control. (**B**) Densitometry quantification of the immunoblot in (**A**). Data are shown as means ± S.E.M. from three independent experiments. #$p < 0.05$, *$p < 0.001$ (ANOVA). (**C**) Fluorescent phalloidin staining of F-actin and immunofluorescent staining of β-catenin and vimentin in ARPE-19 cells treated with the indicated concentrations of $NaIO_3$. White rectangles indicate zoomed area shown in the bottom panel. White arrows indicate the filopodia structures. (**D**) Wound healing assay showing the migration capacity of ARPE-19 cells treated with $NaIO_3$ as indicated. Bottom panel: quantification of the assay. Data are means ± S.E.M. from three independent experiments. #$p < 0.05$, *$p < 0.001$ (ANOVA). (**E**) Experimental outline of *retro*-orbital injection of $NaIO_3$ into mouse eyes. (**F**) H&E staining of the cross-sections of the mouse retinas after the *retro*-orbital injections of $NaIO_3$. ONL - outer nuclear layer, IS - inner segments, OS - outer segments, RPE - retinal pigments epithelium.

get of the NRF2-mediated transcriptional response, was elevated in a concentration-dependent manner with a maximum at 2 mM (Fig. 2**F**). The presence of ROS may interfere with the protein folding and, as a result, trigger the endoplasmic reticulum (ER) stress [52]. Given such close connection between the processes of the oxidative and ER stress, we measured the expression of CHOP, the pro-apoptotic transcription factor involved in the ER stress-related cell death, and an anti-apoptotic factor GRP78, the molecular chaperone involved in protein folding. Indeed, CHOP was significantly upregulated in cells pre-treated with $NaIO_3$, particularly at 2 mM concentration (Fig. 2**F** and **G**). On the other hand, the level of GRP78 was not upregulated (Fig. 2**F** and **G**). It has previously been reported that EGFR activation promotes EMT of RPE cells stimulated by TGF-β1, EGF or cigarette smoke extract [30,53]. In addition, ERK was demonstrated to play the central role in cancer cell EMT [25]. Nevertheless, the role of EGFR and ERK in EMT of RPE cells induced by ROS is still unknown. We demonstrate that the treatment of ARPE-19 cells with $NaIO_3$ resulted in increased phosphorylation of EGFR and ERK in a concentration-dependent manner, indicative of its activation (Fig. 2**H** and **I**).

TGF-β family of cytokines has previously been characterized as the inducers of ROS-stimulated EMT [54]. Therefore, we tested whether the secretion levels of TGF-β1 and BMP4 (TGF-β family member) were affected by the treatment with $NaIO_3$ using ELISA. Interestingly, BMP4 was secreted from ARPE-19 cells under control conditions, however, its secretion was marginally downregulated after the treatment with $NaIO_3$ in a concentration dependent manner (Fig. 2**J**). TGF-β1 secretion from ARPE-19 was extremely low and not affected by $NaIO_3$ stimulation (Fig. 2**K**). The level of EGF, the ligand of EGFR, was also not affected by the treatment with $NaIO_3$ (Fig. 2**L**). These data imply that the multiple signaling pathways are induced by $NaIO_3$ stimulation rather than via the secretion of extracellular factors. To summarize, our results indicate that the treatment of ARPE-19 cells with $NaIO_3$ results in

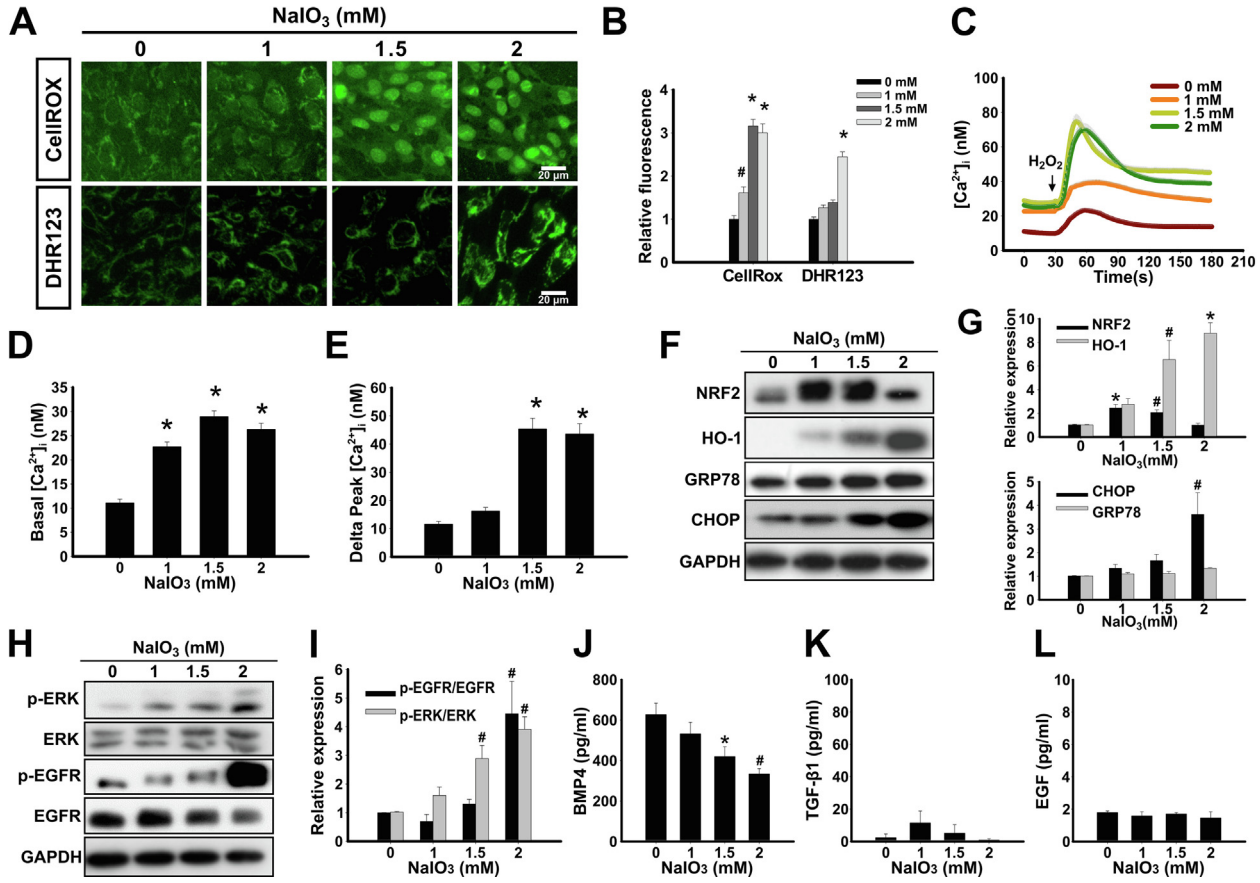

Fig. 2. Characterization of pathway responses to the $NaIO_3$-induced oxidative stress in ARPE-19 cells. (**A**) CellROX and DHR123 fluorescence assays to detect ROS levels in $NaIO_3$-treated ARPE-19 cells. (**B**) Quantification of fluorescence assay in (**A**). Data are presented as mean fluorescence values relative to 0 mM $NaIO_3$. (**C**) Ca^{2+} release profile detected by Fluo-4 AM fluorescent Ca^{2+} indicator with stimulation of H_2O_2 in ARPE-19 cells pre-treated with the indicated concentrations of $NaIO_3$. (**D**) Quantification of the basal level of $[Ca^{2+}]_i$ in (**C**). (**E**) Quantification of the level of Ca^{2+} released from intracellular storage (delta $[Ca^{2+}]$) in (**C**). In (**D**) and (**E**) data are presented as mean concentrations from 80 cells for each group. (**F**) Western blot showing the expression of the oxidative stress responsive factors (NRF2 and HO-1) and ER stress markers (GRP78 and CHOP) in ARPE-19 cells treated with the indicated concentrations of $NaIO_3$. (**G**) Densitometry quantification of the immunoblot in (**F**). (**H**) Western blot showing the expression of ERK and EGFR and their phosphorylated forms (p-ERK and p-EGFR). (**I**) Densitometry quantification of the immunoblot in (**H**). (**F**) and (**H**) GAPDH was used as a loading control. (**J**, **K**, **L**) ELISA analysis of the secretion of BMP4 (**J**), TGF-β1 (**K**) and EGF (**L**). Quantitative data are means ± S.E.M. from three independent experiments. #$p < 0.05$, *$p < 0.01$ (ANOVA).

the elevation of ROS, the increase of basal $[Ca^{2+}]_i$ and intracellular storage of Ca^{2+}, the induction of NRF2-dependent anti-oxidative stress response, the enhancement of ER stress-induced pro-apoptotic transcription factor CHOP, and the activation of ERK and EGFR.

Ca^{2+} signaling, EGFR, and ERK are required for the EMT response of ARPE-19 cells to $NaIO_3$-induced oxidative stress

To further analyze the regulatory role and interplay of $[Ca^{2+}]_i$, p-ERK, and p-EGFR in $NaIO_3$-stimulated EMT, ARPE-19 cells were pre-treated with BAPTA-AM, a Ca^{2+} chelator; erlotinib, an inhibitor of EGFR; or FR180204, an inhibitor of ERK, for 24 h prior to the treatment with $NaIO_3$ (Fig. S1**B**). The treatment of ARPE-19 with these inhibitors per se, without subsequent induction of oxidative stress, did not significantly alter the expression of the analyzed proteins (Fig. 3**A**). As was observed by western blotting, the treatment with $NaIO_3$ increased the level of vimentin and decreased the level of β-catenin, indicative of the induction of the EMT program; increased the levels of NRF2 and HO-1, indicative of the classical oxidative stress response; increased the level of CHOP, indicative of the pro-apoptotic response to the ER stress (Fig. 3**A**). At the same time, both EGFR and ERK were activated by phosphorylation (Fig. 3**A**). However, the pre-treatment with BAPTA-AM, erlotinib or FR180204 resulted in abrogation of these responses to the oxidative stress (Fig. 3**A**). Moreover, the immunofluorescent staining also showed that the pre-treatment of ARPE-19 with all the inhibitors reduced the EMT response of downregulation of β-catenin and upregulation of vimentin, in addition, phalloidin staining of F-actin also revealed the suppression of formation of the mesenchymal cytoskeleton with the presence of filopodia structures (Fig. 3**B**). All the inhibitors significantly reduced the migration capacity of oxidative stress-exposed ARPE-19 cells, which is consistent with suppressing EMT phenotype (Fig. 3**C**). To summarize, all these observations indicate that intact Ca^{2+} signaling, EGFR and ERK are required for the oxidative stress-induced EMT in RPE. At the same time, the inhibition of ERK by FR180204 generally resulted in the most complete and effective abrogation of these oxidative stress-induced pathways leading to EMT.

Post-treatment with FR180204 downregulates $NaIO_3$-induced multiple signaling pathways resulting in EMT

Given that the pre-treatment with ERK inhibitor resulted in the most efficient suppression of the oxidative stress-induced signaling pathways regulating EMT in ARPE-19 cells, we applied post-treatment with FR180204 to dissect the mechanisms of the oxidative stress-induced responses in more detail (Fig. S1**C**).

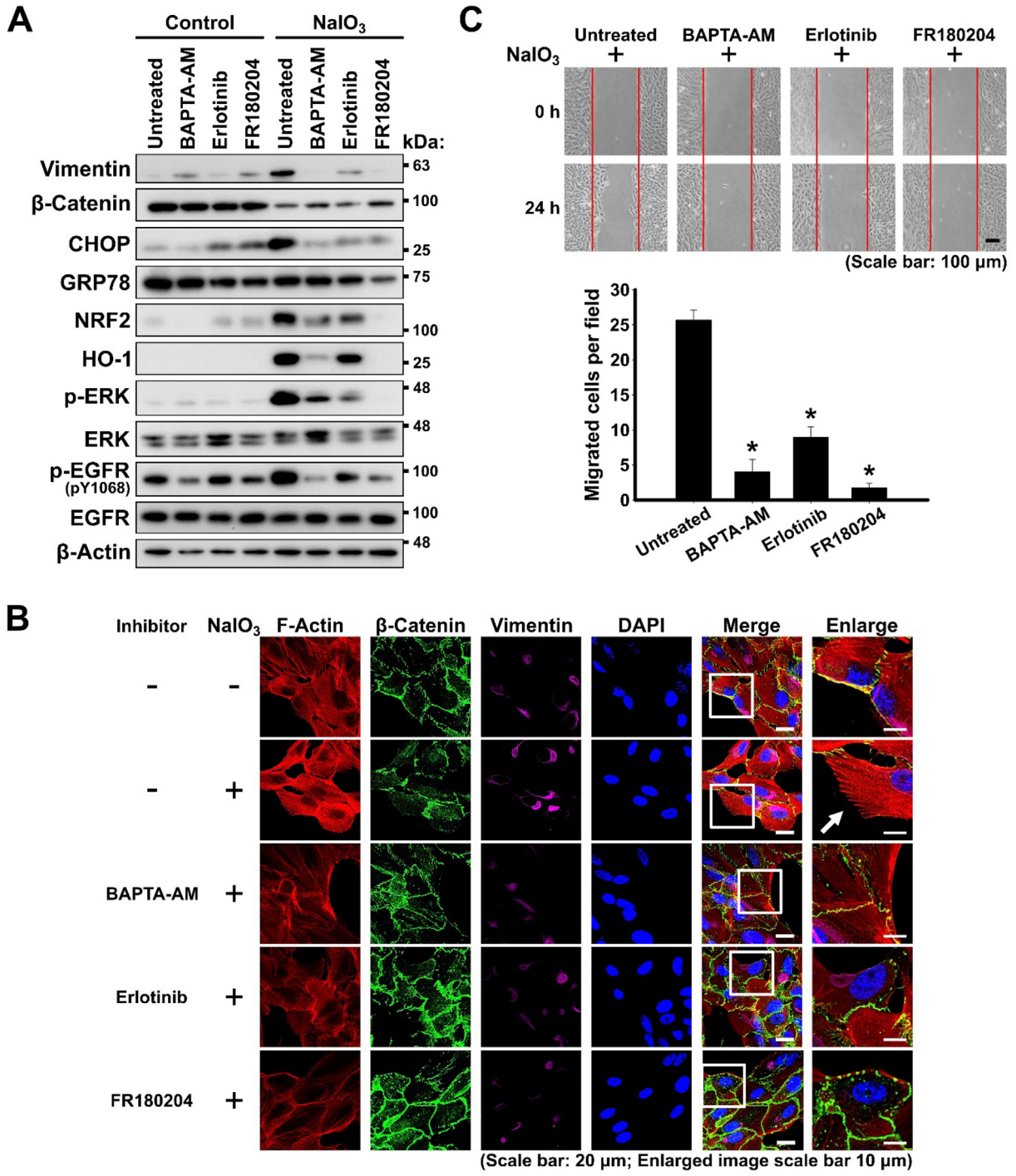

Fig. 3. Ca^{2+} signaling and the activation of ERK and EGFR mediate the EMT response of ARPE-19 cells to $NaIO_3$-induced oxidative stress. (**A**) Western blot analysis of the expression of the indicated proteins in ARPE-19 cells treated or not treated with $NaIO_3$ with or without pre-treatment with the indicated inhibitors. β-Actin – loading control. (**B**) Fluorescent phalloidin staining of F-actin and immunofluorescent staining of β-catenin and vimentin in $NaIO_3$-administrered ARPE-19 cells with or without pre-treatment with the indicated inhibitors. White arrow indicates the filopodia structures. (**C**) Wound healing assay showing the migration capacity of $NaIO_3$-administered ARPE-19 cells pre-treated with the indicated inhibitors. Bottom panel: quantification of the assay. Quantitative data are means ± S.E.M. from three independent experiments. $^*p < 0.001$ (ANOVA).

Surprisingly, the post-treatment of ARPE-19 with FR180204 resulted in the reduction of ROS accumulation from the treatment with $NaIO_3$ (Fig. 4**A and B**). There were no detectable differences in viability and cytotoxicity between $NaIO_3$-stimulated ARPE-19 cells post-treated with FR180204 and untreated controls as shown by CCK-8 and LDH assays, respectively (Fig. S2**C and D**). The $NaIO_3$-stimulated increase of basal level of $[Ca^{2+}]_i$ and the enhancement of Ca^{2+} in intracellular storage were markedly suppressed by post-treatment with FR180204 (Fig. 4**C–E**). The $NaIO_3$-activated NRF2/HO-1 antioxidant signaling pathway and pro-apoptotic transcription factor CHOP were not elicited in cells post-treated with FR180204 (Fig. 4**F**). The induction of vimentin and the reduction of β-catenin did not occur in the cells post-treated with FR180204, indicative of the attenuation of EMT (Fig. 4**G**). The

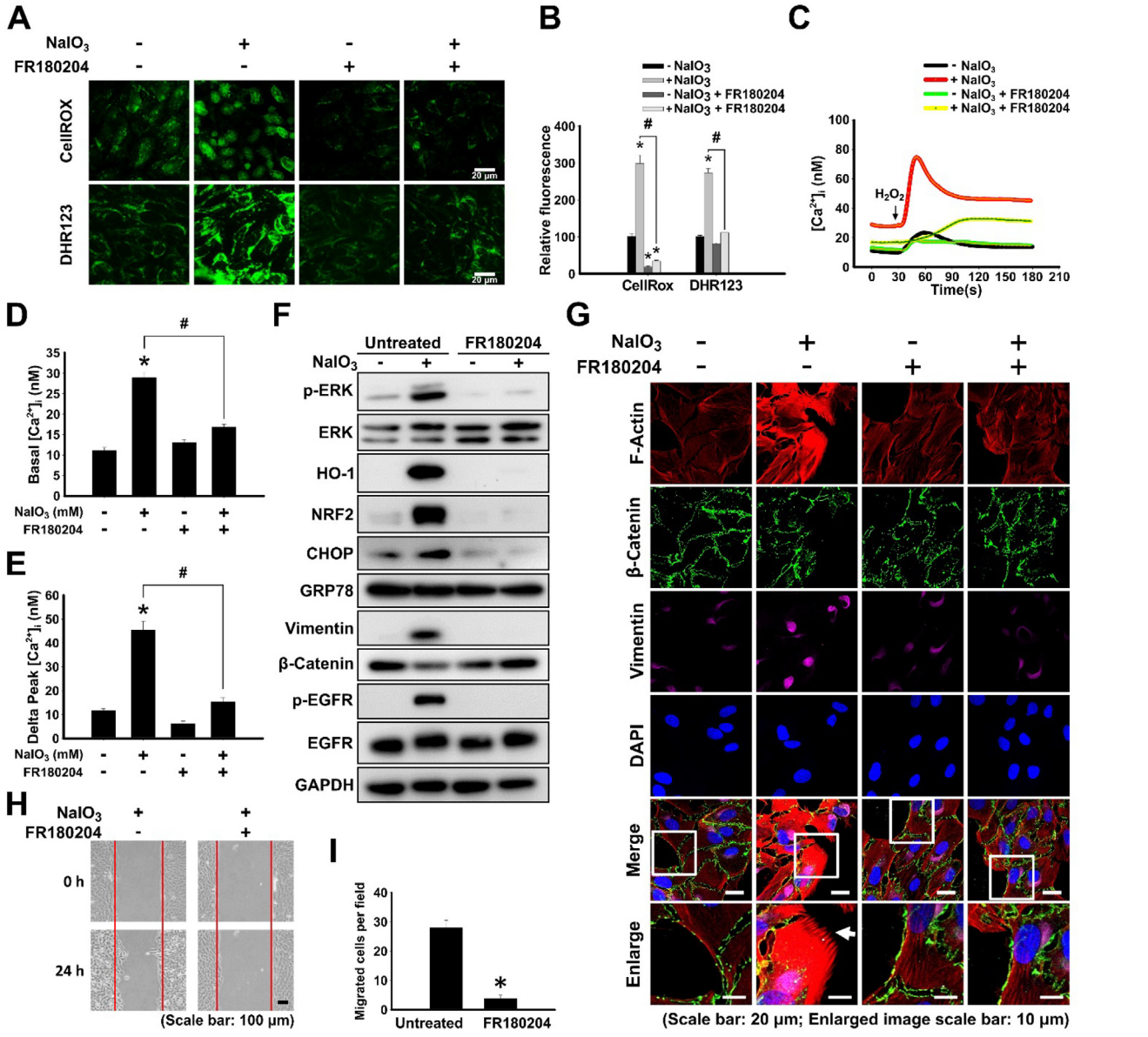

Fig. 4. Post-treatment with FR180204 downregulates $NaIO_3$-induced multiple signaling pathways resulting in EMT. (**A**) CellROX and DHR123 fluorescence assays to detect ROS levels in 2 mM $NaIO_3$-treated ARPE-19 cells with or without post-treatment with 10 μM FR180204. (**B**) Quantification of fluorescence assay in (**A**). (**C**) $[Ca^{2+}]_i$ release profile detected by Fluo-4 AM fluorescent Ca^{2+} indicator with stimulation by H_2O_2 in 2 mM $NaIO_3$-treated ARPE-19 cells in the absence or presence of post-treatment with FR180204. (**D**) Quantification of the basal level of $[Ca^{2+}]_i$ in (**C**). (**E**) Quantification of the level of released $[Ca^{2+}]_i$ (delta peak) in (**C**). In (**D**) and (**E**) data are presented as mean concentrations from 80 cells for each group. (**F**) Western blot showing the expression of the oxidative stress responsive factors (NRF2 and HO-1), ER stress markers (GRP78 and CHOP), EMT markers (vimentin and β-catenin), p-ERK and p-EGFR in ARPE-19 cells administered with $NaIO_3$ in the absence or presence of post-treatment with FR180204. GAPDH – loading control. (**G**) Fluorescent phalloidin staining of F-actin (red) and immunofluorescent staining of β-catenin (green) and vimentin (purple) of $NaIO_3$-treated ARPE-19 cells with or without post-treatment with FR180204. (**H**) Wound healing assay showing the motility of $NaIO_3$-treated ARPE-19 cells with or without post-treatment with FR180204. (**I**) Quantification of the number of migrated cells (N = 3, $^*p < 0.01$ vs. 0 mM $NaIO_3$ (Student's-test). (For interpretation of the references to colour in this figure legend, the reader is referred to the web version of this article.)

activation of ERK and EGFR was also suppressed by the post-treatment with FR180204. The $NaIO_3$-activated migration capacity of ARPE-19 was suppressed by the post-treatment with FR180204 (Fig. 4**H** and **I**). Furthermore, the suppression of the $NaIO_3$-activated EMT by post-treatment with FR180204 was also confirmed with F-actin staining that revealed the diminished intensity and the absence of filopodia structures (Fig. 4**G**). To summarize, all these observations indicate that post-treatment with FR180204 decreases ERK activation resulting in the reduced intracellular ROS and $[Ca^{2+}]_i$, downregulated ER stress markers expression and EGFR phosphorylation, and attenuated $NaIO_3$-induced EMT of RPE cells.

ERK plays a critical role in promoting oxidative stress-induced EMT of ARPE-19 cells in contrast to MEK

MEK is the major upstream kinase responsible for the activation of ERK in the MAPK/ERK pathway. We observed that MEK was activated by phosphorylation in response to the treatment with $NaIO_3$ in a concentration-dependent manner (Fig. 5**A**). To study the functional effect of MEK in response to ERK-regulated EMT, we applied post-treatment with U0126 to inhibit MEK activity in $NaIO_3$-administered ARPE-19 cells. Our results demonstrated that the induced p-ERK was decreased by U0126 administration, however, the $NaIO_3$-enhanced HO-1, CHOP, p-EGFR, and EMT markers were

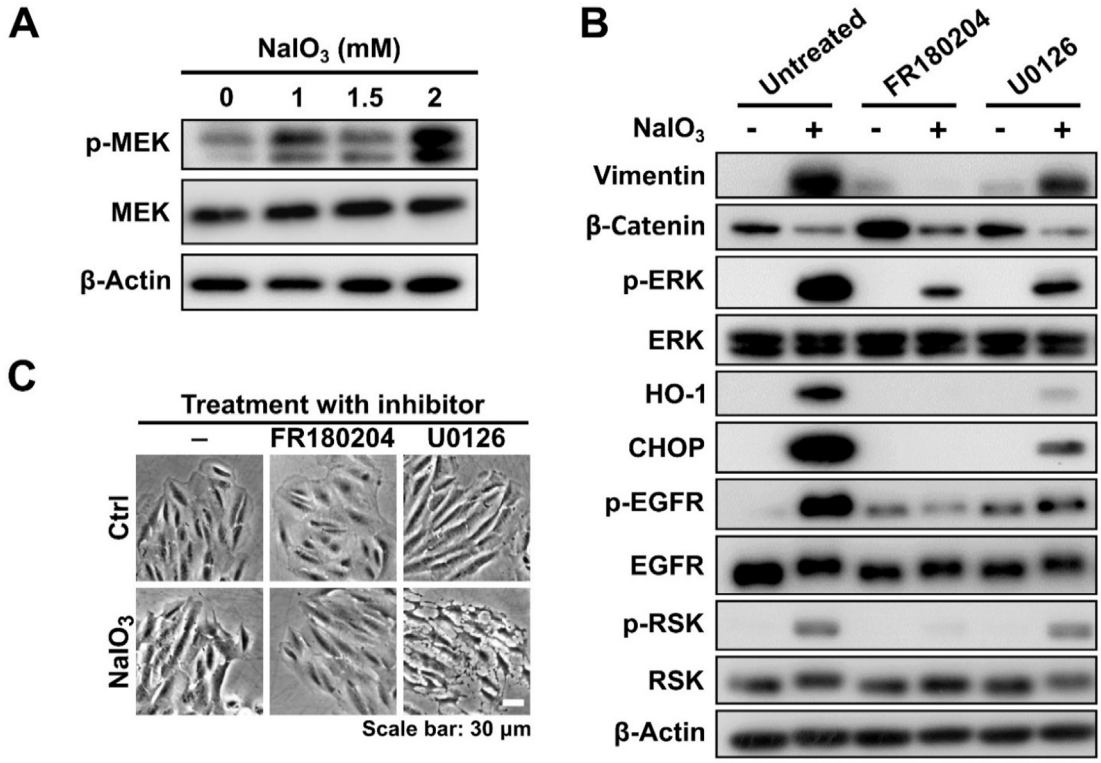

Fig. 5. ERK, rather than MEK, plays a critical role in promoting oxidative stress-induced EMT in ARPE-19 cells. **(A)** Western blot showing the expression of p-MEK and MEK in ARPE-19 cells treated with the indicated concentrations of $NaIO_3$. (**B**) Western blot showing the expression of the indicated markers in ARPE-19 cells treated with $NaIO_3$ with or without the post-treatment with FR180204 or U0126. β-Actin in (**A**) and (**B**) was used as a loading control. (**C**) Bright-field images of ARPE-19 cells treated or not treated with $NaIO_3$ in the absence or presence of the post-treatment with FR180204 or U0126.

partially downregulated by U0126, albeit not as robustly as by FR180204 (Fig. 5**B**). When the cells were examined by bright-field microscopy, it was clearly observed that the treatment with $NaIO_3$ resulted in the loss of an epithelial morphology with smooth edges and close contacts between cells (Fig. 5**C**). When the cells were post-treated with FR180204, but not U0126, the epithelial phenotype was preserved, however, the post-treatment with U0126 was associated with the obvious cell membrane damage and morphology change in $NaIO_3$-stimulated cells (Fig. 5**C**). It implies that MEK, the upstream kinase of ERK, plays a role not only in the progression of EMT through ERK activation, but also in a survival signaling for $NaIO_3$-treated ARPE-19 cells. On the other hand, the family of p90 ribosomal S6 kinases (RSKs), which are downstream of ERK, have been revealed to be important mediators of ERK signaling, and were demonstrated to downregulate cell–cell contact and increase cellular migration [55]. Our results showed that p-RSK was decreased by post-treatment with FR180204, but not with U0126 (Fig. 5**B**). It suggests that ERK regulates oxidative stress-induced EMT via RSK activation in ARPE-19 cells.

RNA-Seq profiling of gene expression upon ERK inhibition in $NaIO_3$-stimulated RPE cells

To investigate the effect of FR180204 on $NaIO_3$-induced oxidative stress on a transcriptome-wide level, we performed RNA-Seq analysis of the transcriptomes of ARPE-19 cells treated with $NaIO_3$ in the absence or presence of FR180204. ARPE-19 cells were pre-treated with 0, 1, or 1.5 mM $NaIO_3$ followed by treatment with 10 μM FR180204 in a fresh medium for 24 h before harvesting total RNA. The principal component analysis (PCA) revealed that the treatment of ARPE-19 cells with FR180204 *per se* without the application of oxidative stress did not result in any significant changes in global gene expression (Fig. 6**A**). On the other hand, the first variance component (PC1) effectively separated the samples treated with $NaIO_3$ in the absence of FR180204, and the second variance component (PC2) accounted for the effect of FR180204 in $NaIO_3$-treated samples (Fig. 6**A**). However, PC1 values of FR180204-treated samples were closer to those of $NaIO_3$-untreated samples, implying that ERK inhibition could partially reverse the effect of $NaIO_3$ (Fig. 6**A**). Therefore, in our differential gene expression analysis, we aimed to identify the genes whose differential expression caused by $NaIO_3$ treatment could be reversed by concomitant FR180204 treatment. First, we identified the genes upregulated and downregulated by $NaIO_3$ treatment *per se* (Fig. 6**B**, top panel), as well as those regulated by concomitant treatment with $NaIO_3$ and FR180204 (Fig. 6 **B**, bottom panel). Remarkably, by applying the genes differentially regulated by both 1 and 1.5 mM $NaIO_3$ with more than two-fold change (Fig. 6**B**) to STRING protein–protein interaction network analysis, we found that many of them were centered in a network regulated by β-catenin (CTNNB1) (Fig. S4A). On the other hand, the genes differentially regulated by FR180204 treatment were centered around histone deacetylase 1 (HDAC1) (Fig. S4**B**). Further, we contrasted the lists of genes upregulated by the treatment with 1.5 mM $NaIO_3$ *per se* and downregulated in the cells treated with 1.5 mM $NaIO_3$ +- FR180204 and found that they were both enriched with Gene Ontology (GO) terms related to oxidative stress response, Ca^{2+} signaling and EMT (Fig. 6**C and D**). On the contrary, the list of genes downregulated by the treatment with 1.5 mM $NaIO_3$ and upregulated in 1.5 mM $NaIO_3$ + FR180204 sample were enriched in the GO terms related to calcium signaling, EMT, stem cell/aging and amyloid-beta metabolism (Fig. 6**E and F**). As shown in clustering

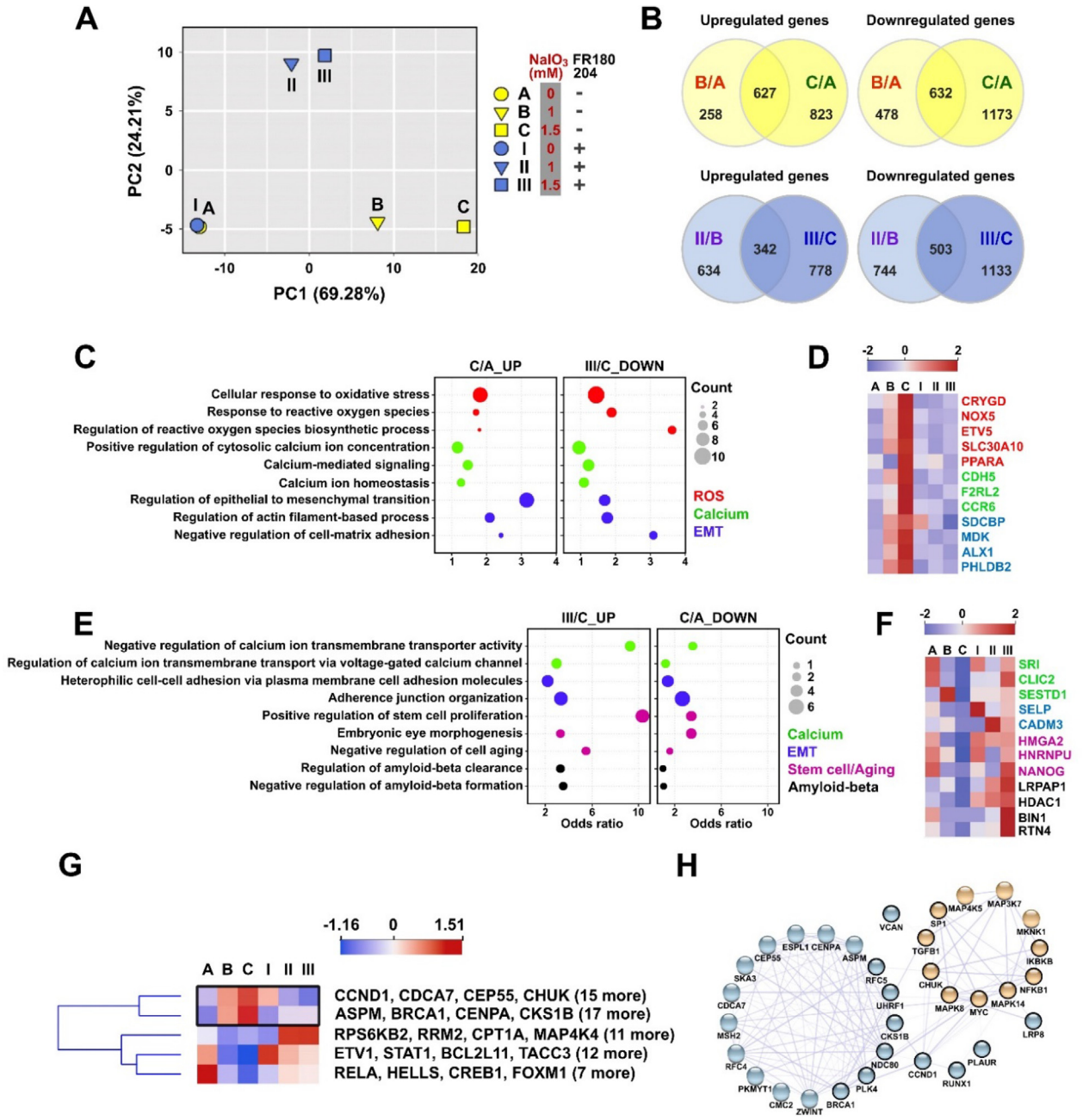

Fig. 6. RNA-Seq profiling of gene expression in $NaIO_3$-administered ARPE-19 cells upon ERK inhibition. (**A**) PCA plot showing the difference of global gene expression in ARPE-19 cells administered with $NaIO_3$ and post-treatment with FR180204 as indicated. (**B**) Venn diagrams showing the numbers of unique and common differentially expressed genes in the indicated experimental groups. (**C**) Bubble plot showing the significantly enriched GO terms of the upregulated genes (1.5 mM $NaIO_3$ treatment) and the downregulated genes (FR180204 post-treatment) in ROS (red), Ca^{2+} (green), and EMT (blue). (**D**) Clustering heatmap diagram of the genes differentially expressed in (**C**). (**E**) Bubble plot showing the significantly enriched GO terms of the upregulated genes in cells administered with 1.5 mM $NaIO_3$ following post-treatment with FR180204 and the downregulated genes in 1.5 mM $NaIO_3$-administered cells. (**F**) Clustering heatmap diagram of the genes differentially expressed in (**E**). (**G**) Clustering heatmap diagram of the genes upregulated in the $NaIO_3$-administered ARPE19 cells and downregulated by following post-treated with FR180204 (top cluster, black rectangle), and the genes with opposite regulation pattern (bottom cluster). (**H**) STRING protein–protein interaction network implicated in MAPK/ERK (yellow) and EMT (blue) signaling. (For interpretation of the references to colour in this figure legend, the reader is referred to the web version of this article.)

heatmaps, the expression of five ROS response-associated genes (*CRYGD*, *NOX5*, *ETV5*, *SLC30A10*, and *PPARA*), three Ca^{2+} signaling-associated genes (CDH5, F2RL2, and CCR6), and four EMT-associated genes (*SDCBP*, *MDK*, *ALX1*, and *PHLDB2*) was gradually increased in response to $NaIO_3$ treatment (Fig. 6**D**). The heatmap showed that the expression of three Ca^{2+} signaling-associated genes (*SRI*, *CLIC2*, and *SESTD1*), two EMT-associated genes (*SELP* and *CADM3*), three stem cell-associated genes (*HMGA2*, *HNRNPU*, and *NANOG*), and four amyloid-beta-associated genes (*LRPAP1*, *HDAC1*, *BIN1*, and *RTN4*) were gradually increased in response to FR180204 treatment (Fig. 6**F**). Based on the known EMT and MAPK-associated genes from the GSEA database, we clustered the genes according to their expression in our RNA-Seq data. The clustered heatmap revealed the significantly upregulated genes upon $NaIO_3$ treatment that were significantly downregulated by FR180204 co-treatment (Fig. 6**G**). In such a way, we identified forty genes including CCND1, CDCA7, CEP55, CHUK, ASPM, BRCA1, CENPA, NCKS1B, and others (Fig. 6**G**). By using the STRING pro-

tein–protein interaction database, we constructed the relationship of these top-ranking genes in the MAPK and EMT signaling (Fig. 6**H**). According to the network, we found that *CCND1* was closely connected to both EMT and MAPK signaling and was a subject of a significant change after FR180204 treatment, suggesting that it could be a crucial mediator of the effects of ERK inhibition (Fig. 6**H**). The transcripts per million (TPM) values and Z-scores of the transcripts implicated in EMT and MAPK signaling are shown in **Supplementary Table 2**.

FR180204 prevents $NaIO_3$-induced p-ERK-mediated remodeling in the mouse retina

To characterize the effects of FR180204 on the retina, mice were *retro*-orbitally injected with 100 nM, 500 nM, or 10 μM FR180204. As was shown by H&E staining of the eye cross sections, no significant adverse effect on the morphology and thickness of the retina was observed in mice treated with the indicated concentrations of FR180204 (Fig. 7**A**). As was shown by OCT, there were no detectable hyperreflective foci (HRF) found in the retinas administered with 100 nM FR180204, however, some HRF were found in the retinas administered with 10 μM FR180204 (Fig. 7**B**). Therefore, we decided to treat mice with 100 nM FR180204 by *retro*-orbital injection in the following experiments. Moreover, to confirm the role of ERK in the oxidative stress-mediated EMT *in vivo*, we delivered $NaIO_3$ to the mice by IP injection as described previously [42] (Fig. 7**C**). On the next day, 100 nM FR180204 was delivered to the right eye by *retro*-orbital injection in parallel with the control injection of DMSO in PBS to the left eye. On the 7th day, the mice were sacrificed and the whole mount retinas were analyzed (Fig. 7**C**). As was shown by immunostaining of tight junctions (ZO-1 protein), the administration of $NaIO_3$ resulted in the disturbed structure of the epithelium with loose borders between individual RPE cells. This effect was accompanied by increased phosphorylation of ERK. Interestingly, the FR180204 post-treatment clearly resulted in the preservation of the intact structure of RPE with low ERK phosphorylation level (Fig. 7**D**). The same experimental design was applied in parallel to ARPE-19 cell culture as a control, and we observed p-ERK fluorescence intensity increase after $NaIO_3$ stimulation, which was reduced by FR180204 post-treatment (Fig. 7**E**). Importantly, FR180204 post-treatment restored the reduction of ZO-1 in the retina (Fig. 7**D**) and decreased F-actin induction in ARPE-19 cells stimulated by $NaIO_3$ (Fig. 7**E**), which implied that FR180204 might diminish the $NaIO_3$-induced degeneration of RPE cells. To summarize, we observed the *in vivo* effect of FR180204 on p-ERK-associated RPE cell EMT induced by oxidative stress, which was consistent with *in vitro* findings.

FR180204 prevents $NaIO_3$-induced structural changes in the mouse retina

To further characterize the effects of FR180204 on the consequences of $NaIO_3$-induced oxidative stress *in vivo*, we administered $NaIO_3$ *retro*-orbitally (the same procedure as in Fig. 1**E and 1F**) followed by *retro*-orbital injection of FR180204 on the next day (Fig. 8**A**). After three days, we examined the H&E-stained whole eye cross sections and detected the $NaIO_3$-induced upward translocation of RPE cells from the RPE layer and distortion of the adjacent retinal layers (Fig. 8**B**). The post-treatment with FR180204, on the other hand, clearly prevented these effects (Fig. 8**B**). To investigate more long-term effects of FR180204 on $NaIO_3$-induced oxidative stress *in vivo*, different concentrations of $NaIO_3$ were administered intraperitoneally followed by *retro*-orbital injection of FR180204 into the right eye and DMSO control into the left eye on the next day. The mice were sacrificed after one week and 6 weeks and the cross sections were analyzed by H&E staining (Fig. 8**C**). After seven days post-injection with 20 or 30 mg/ml of $NaIO_3$, the diffusion of RPE cells and distortion of retinal structure were observed (Fig. 8**D**). However, the post-treatment with FR180204 noticeably alleviated these effects, particularly at lower concentration of $NaIO_3$ (20 mg/ml). Moreover, the total area of the retina affected by $NaIO_3$-induced structural perturbations was significantly reduced upon FR180204 post-treatment. In the case of 6 weeks after administration of $NaIO_3$, we observed the significant thinning of the retina, indicative of a heavy permanent loss of a substantial number of retina cells. In comparison, the treatment with FR180204 resulted in preservation of relatively intact structure of the retina (Fig. 8**D**). In conclusion, we observed that post-treatment with FR180204 alleviated both transient and long-term irreversible damage to the retina caused by $NaIO_3$.

FR180204 reduces $NaIO_3$-induced retinal lesion as observed by SD-OCT

To further validate the effect of $NaIO_3$ on the rodent retina and the rescue role of FR180204, we applied a non-invasive imaging method, spectral domain optic coherence tomography (SD-OCT), which produces high-resolution volumetric histological images of the retina. We observed the SD-OCT images from the posterior eye of mouse after $NaIO_3$ and FR180204 administration performed as described above (Fig. 8**C**). The SD-OCT cross-sectional and en face images showed that the retina lesion and HRF were observed in the retina at day 7 after 30 mg/ml $NaIO_3$ injection (Fig. 9**A and B**). Moreover, after 30 mg/ml $NaIO_3$ injection, the retina structure was generally thinner compared to the control, and HRF were observed in both the vitreous and the retina (Fig. 9**A**). However, the number of HRF was significantly decreased upon FR180204 post-treatment (Fig. 9**A–C**). In addition, the SD-OCT cross-sectional images showed that the retina was subjected to lesion and its thickness was reduced as a result of 30 mg/ml $NaIO_3$ injection after 6 weeks. However, the thicker retina and the outer plexiform layer (OPL) could be observed in the retina post-treated with FR180204 (Fig. 9**D**). These results suggested that the treatment with FR180204 alleviated the retinal lesions triggered by $NaIO_3$-induced oxidative injury in a short term (7 days) and a long term (6 weeks), which was consistent with the histological observations (Fig. 7).

Discussion

Oxidative stress is one of the most important pathogenesis factors in AMD. RPE cells are subjected to particularly high oxidative cellular environment due to physiological sources of oxidative stress such as high metabolic activity of RPE cells [3] and the phagocytosis of photoreceptor outer segments [4], as well as unique sources of photooxidative stress induced by high UV exposure [56,57]. In addition, lifestyle-associated factors including tobacco smoking contribute to oxidative stress-related RPE cell damage in AMD progression [30,58]. Indeed, degenerative RPE cells are exposed to particularly high accumulation of ROS resulted from the decreased capacity to neutralize ROS and diminished autophagy ability associated with aging [5]. In previous studies, it has been shown that $NaIO_3$ increases the level of ROS and generates cellular oxidative stress to harm RPE cells, thus it can be used to investigate the pathogenesis of AMD [15,18]. In our study, we applied the experimental conditions to induce intracellular oxidative stress that is implicated in AMD etiology by administering the sublethal concentrations of $NaIO_3$ *in vitro* and *in vivo*. In previous studies, the programmed cell death of RPE cells occurring by the mechanisms of apoptosis [59,60] or necroptosis [15] was the major $NaIO_3$-induced effect investigated as the causative factor of AMD.

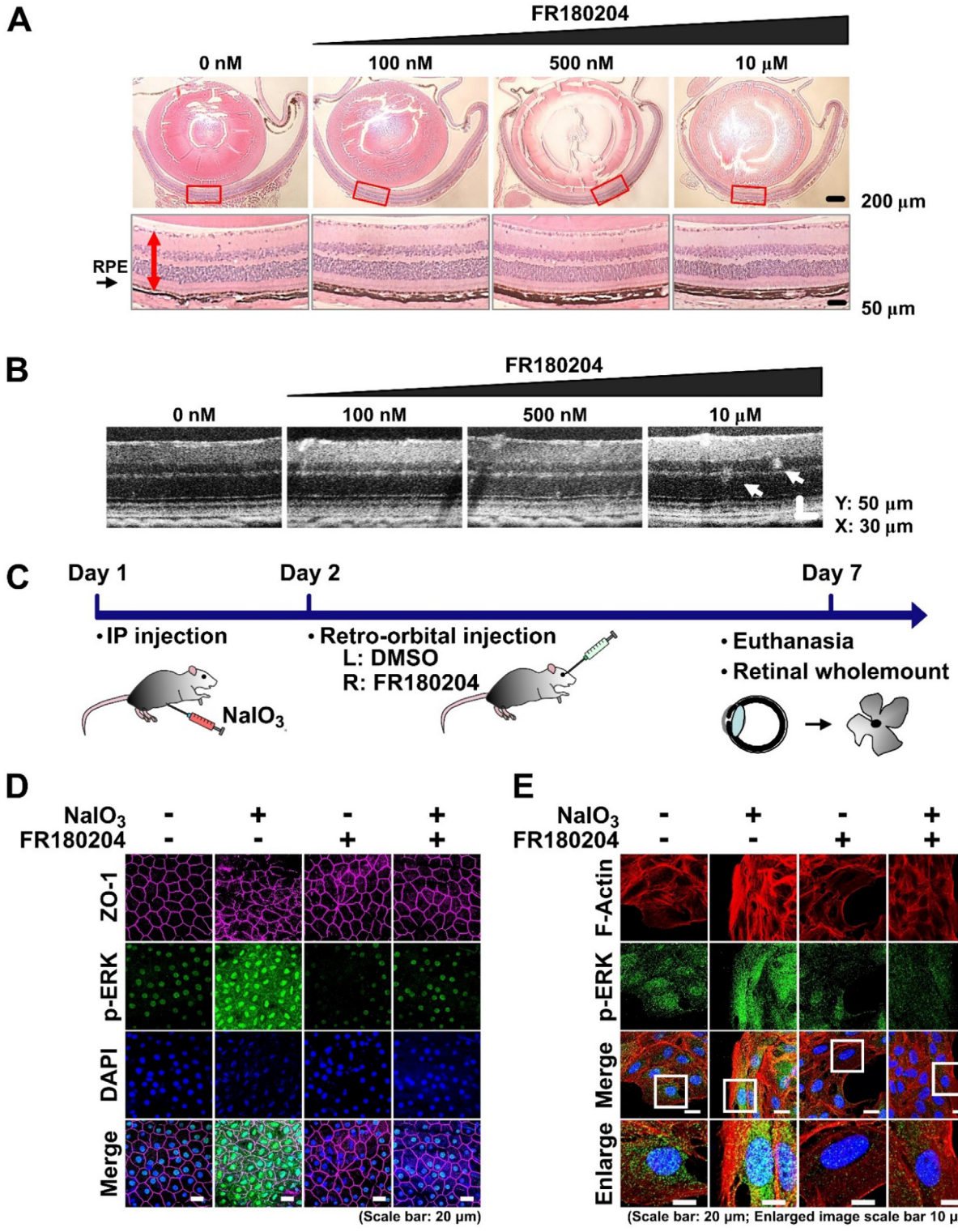

Fig. 7. FR180204 prevents EMT of RPE cells. **(A)** H&E staining of whole eye cross sections (top panel) and zoomed retina segments marked by red rectangles (bottom panel) of mice treated with the indicated concentrations of FR180204 using *retro*-orbital injection. Red arrows indicate thickness of the retina. **(B)** SD-OCT images of the mouse retinas treated with the indicated concentrations of FR180204 using *retro*-orbital injection. **(C)** Experimental outline to investigate the effect of FR180204 on $NaIO_3$-induced EMT *in vivo*. (**D**) Immunostaining of the retinal wholemounts subjected to the indicated treatments with antibodies against ZO-1 and p-ERK. (**E**) Immunostaining of ARPE-19 cells subjected to the indicated treatments with phalloidin antibodies against F-actin and p-ERK. In (**B**) and (**C**) nuclei stained with DAPI. (For interpretation of the references to colour in this figure legend, the reader is referred to the web version of this article.)

In our study, we applied an *in vitro* model based on ARPE-19 cells treated with the lower concentration range of $NaIO_3$ (0–2 mM), which resulted in the induction of EMT (Fig. 1) as well as the activation of multiple important signaling pathways (Fig. 2), but did not lead to substantial cell death (Fig. S2A and B). In such conditions, we clearly observed that ARPE-19 cells underwent the transition from epithelial to mesenchymal phenotype as was observed by the expression of EMT markers (Fig. 1A) and the loss of epithe-

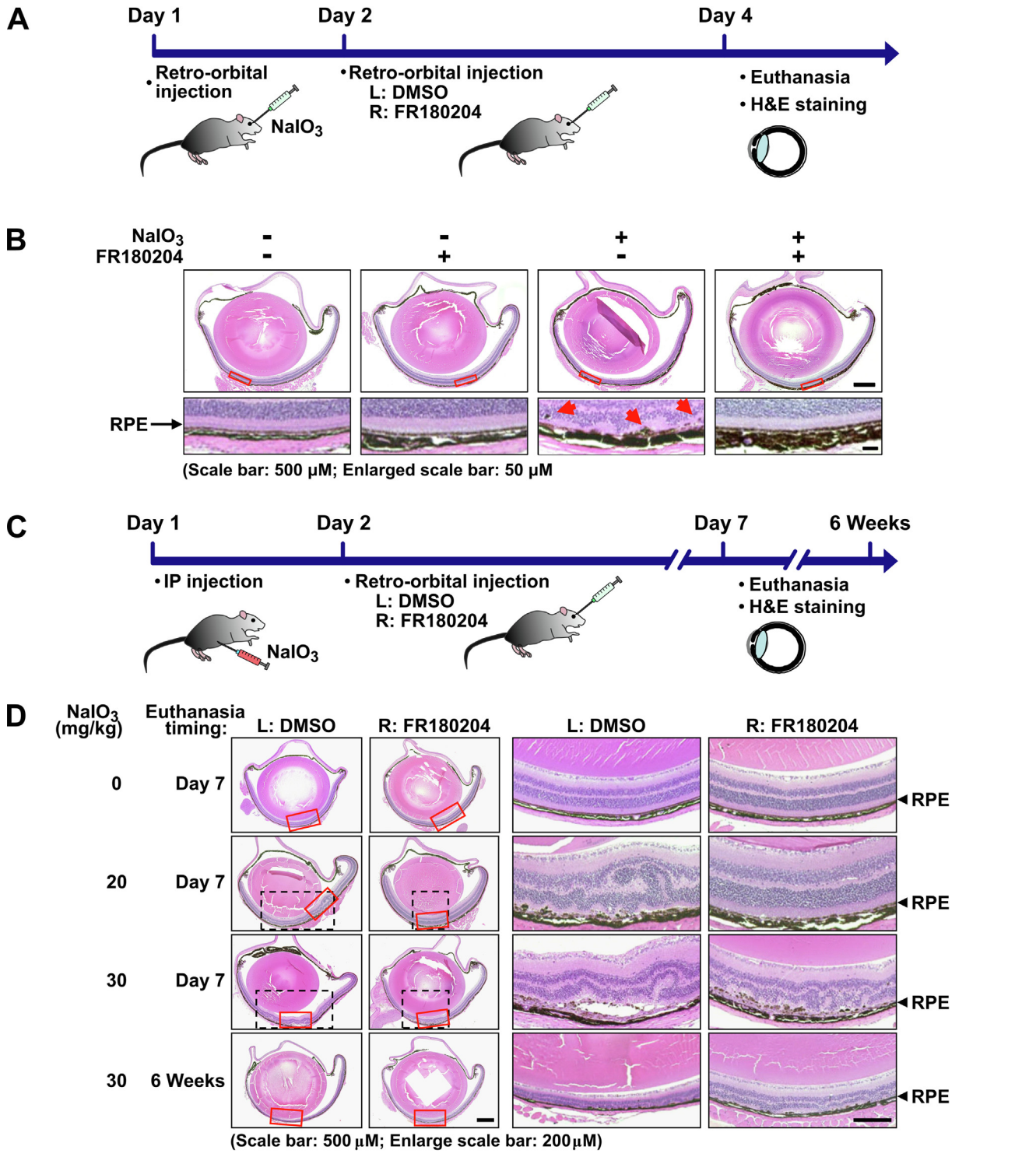

Fig. 8. FR180204 restores $NaIO_3$-induced structural changes in the mouse retina. (**A**) and (**C**) Schemes of experimental design for (**B**) and (**D**), respectively. (**B**) H&E staining of whole eye cross sections (top panel) and zoomed retina segments marked by red rectangles (bottom panel). Red arrows indicate diffusing RPE cells. (**D**) H&E staining of whole eye cross sections (left panels) and zoomed retina segments marked by red rectangles (right panels). Dashed black rectangles show total area of the retina with discernible perturbations. (For interpretation of the references to colour in this figure legend, the reader is referred to the web version of this article.)

lial phenotype (Fig. 1C). Moreover, such oxidative stress conditions increased RPE cell motility and clearly disturbed retinal structure *in vivo* when $NaIO_3$ was delivered to the mouse eyes (Fig. 1E).

The cigarette smoke extract [30], TGF-β1 [53,61], and EGF [30] were used as the sources of oxidative stress to induce EMT and study the regulatory networks in RPE cells as the models for AMD. The increase of ROS levels is known to initiate various signaling pathways that can result in the activation of EMT-specific transcription factors [62,63]. In this study, the level of secreted TGF-β1 was negligible and BMP4 was decreased upon $NaIO_3$ treatment in our ARPE-19 experimental system (Fig. 2H and I). Therefore, according to our experimental conditions, the oxidative stress-related signaling pathways and EMT are directly induced by oxidative stress rather than TGF-β1 or BMP4 in ARPE-19 cells. Impor-

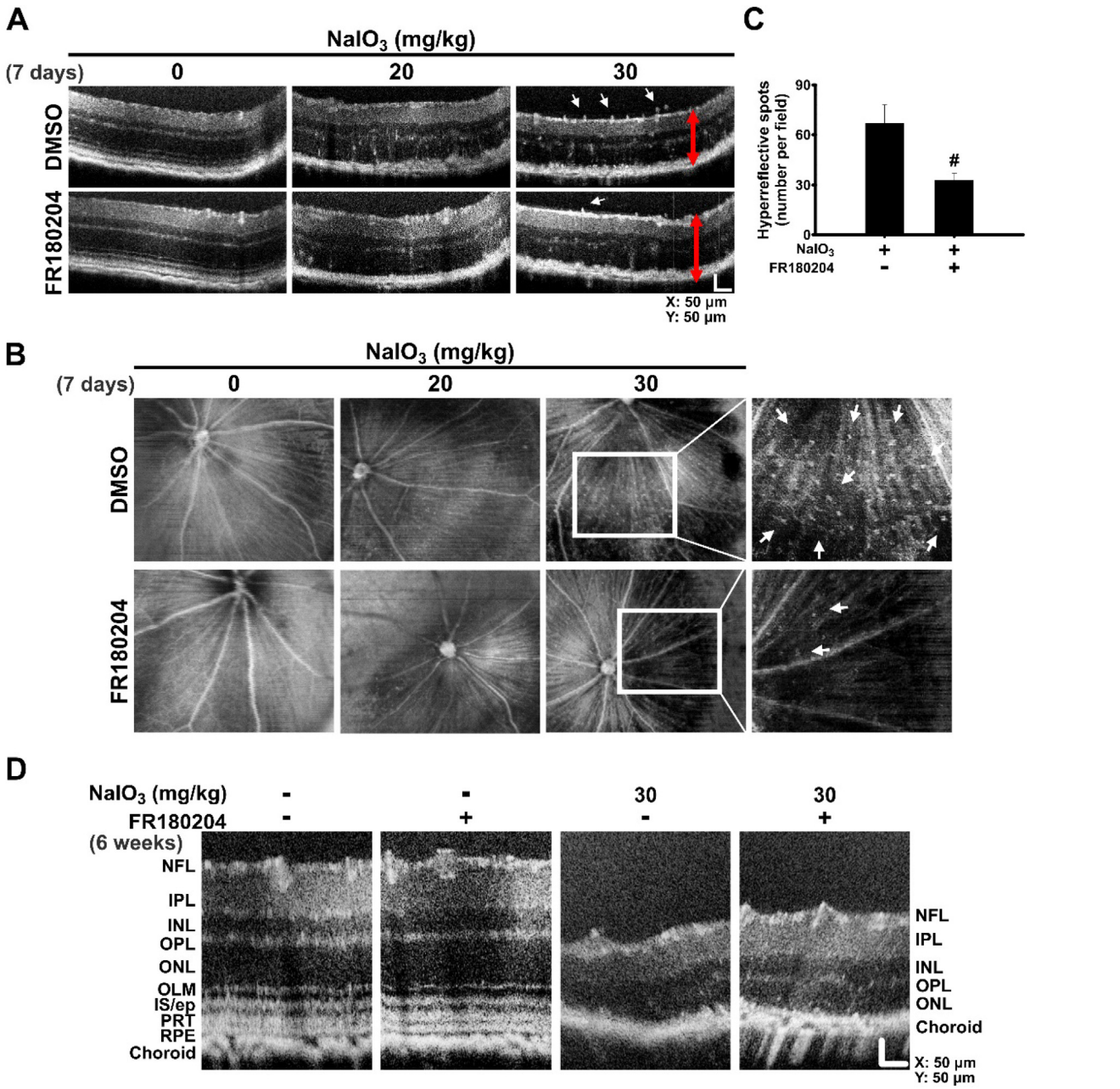

Fig. 9. FR180204 reduces $NaIO_3$-induced retinal lesion as observed by SD-OCT. Cross-sectional (**A**) and en face (**B**) SD-OCT images of the $NaIO_3$-administered mouse retinas with or without FR180204 post-injection 7 days after the indicated treatment. White arrows show hyperreflective foci (HRF). Red arrows indicate the thickness of the retina. (**C**) Quantification of HRF in (**B**). N = 3, #$p < 0.05$ (ANOVA). (**D**) Cross-sectional SD-OCT images showing the retinal structures 6 weeks after the indicated treatment. NFL, nerve fiber layer; IPL, inner plexiform layer; INL, inner nuclear layer; OPL, outer plexiform layer; ONL, outer nuclear layer; OLM, Outer Limiting Membrane; IS/ep, inner segment/ellipsoid layer; PRT, photoreceptor tip layer. (For interpretation of the references to colour in this figure legend, the reader is referred to the web version of this article.)

tantly, previously it has been demonstrated that TGF-β1 is unable to initiate EMT in porcine RPE cells [9], though TGF-β1 is comprehensively used as a classic inducer of EMT. Besides, the role of EGFR-mediated signaling pathway was demonstrated in cigarette smoke extract-activated mesenchymal ARPE-19 cells [30], which is consistent with our results showing that erlotinib has a partial effect to attenuate $NaIO_3$-activated multiple pathways, including EMT. Interestingly, the phosphorylation of EGFR at Tyr1068 was induced dramatically by 2 mM $NaIO_3$ (Fig. 2H) but no EGF released into the medium was observed (Fig. 2L), which may be indicative of an unidentified mechanism for EGFR activation related to oxidative stress-induced EMT in ARPE-19 cells.

According to our results, the treatment of ARPE-19 cells with $NaIO_3$ caused a complex cell response characterized by the induction of the core oxidative stress response genes, stimulation of ER stress response, as well as the activation of ERK (Fig. 2 and Fig. 5). Importantly, we also observed the remodeling of Ca^{2+} signaling system as was inferred from the increased basal levels of Ca^{2+} and increased responsiveness to intracellular Ca^{2+} storage (Fig. 2-C-E). Indeed, overwhelming evidence indicates that ROS can induce dynamic changes in $[Ca^{2+}]_i$ and internal amount of Ca^{2+} pool [64] in a variety of cell types [65]. ROS induces and regulates Ca^{2+} signaling via a complex machinery including voltage-dependent Ca^{2+} channels (VDCCs), ryanodine receptors (RyR), 1,4,5-inositol-

triphosphate receptors (IP3R) or other Ca^{2+} pumps and Na^{+}/Ca^{2+} exchangers [65]. All the evidence is consistent with our observations on the robust remodeling of Ca^{2+} signaling system in response to the oxidative stress.

According to our results, $NaIO_3$ induces ERK activation in ARPE-19 cells (Fig. 2**H, 2I, and 6E**) and in RPE cells of the mouse retina (Fig. 7**D**). A clinical study revealed that ERK activity increased in the RPE of patients suffering from geographic atrophy (GA), as well as in a DICER1-depleted mouse model with the characteristics of RPE degeneration [66]. By applying the inhibitors of Ca^{2+} signaling, EGFR/ERK pathway, we identified that among them, FR180204, the specific inhibitor of ERK, induced the most efficient suppression of EMT-related pathways in $NaIO_3$-stimulated ARPE-19 cells (Fig. 3). We found that the suppression of ERK activation by FR180204 ameliorated the EMT of RPE cells and benefited the maintenance of the integrity of the retina stimulated with 20 mg/kg $NaIO_3$ (Fig. 7). A recent study showed that the inhibition of ERK activation in stressed Müller cells of mice exposed to photooxidative stress resulted in the prevention of photoreceptor degeneration [67]. These findings are suggestive of an important role of ERK in retinal degeneration, which supports the idea of ERK inhibition as a possible therapeutic target. In addition, the activation of ERK was found to contribute to retina maturation and was proposed to play a survival role during retinal development [68]. ERK was completely depleted by conditional knockout of *Erk1* and *Erk2* genes in the mouse RPE, which led to diminished RPE65 expression and induced retinal degeneration [69]. These studies support the concept that the ERK signaling pathway has multiple roles, and the activation of ERK in RPE cells is tightly regulated. On the other hand, MEK is the major upstream kinase responsible for the activation of ERK. Unexpectedly, we found that the post-treatment with U0126, a MEK inhibitor, in $NaIO_3$-stimulated ARPE-19 cells resulted in cell membrane damage and morphology change, in contrast to the treatment with FR180204, which restored normal cell morphology (Fig. 5). However, this result is consistent with the clinical research, in which cancer patients administered with MEK inhibitor chemotherapy such as MEK162 and trametinib were found to be affected by ocular toxicity [70,71]. Taken together, these results implied that MEK may play an important role in RPE cell survival signaling pathway compared to ERK.

The pre-treatment with N-acetyl-L-cysteine (NAC) [72] or resveratrol [73], as well as the overexpression of peroxiredoxin 6 (PRDX6) [74], an antioxidant protein, have been found to protect ARPE-19 cells from oxidative stress; besides, the pre-treatment with TGF-β-activated kinase 1 (TAK1) inhibitor, SB431542, was revealed to diminish TGF-β1-induced EMT in ARPE-19 cells [75]. On the other hand, FR180204 is a selective inhibitor of ERK that has been demonstrated to improve collagen-induced rheumatoid arthritis in mice [76] and decrease the viability of combination-treated cancer cells [77,78]. In this study, we treated ARPE-19 cells with FR180204 at 10 μM to inhibit ERK activity [31,32], and found that there were no detectable viability and cytotoxicity differences between the presence and absence of FR180204 administration in $NaIO_3$-stimulated ARPE-19 cells using CCK-8 and LDH analysis **(**Fig. S3**A and** Fig. S3**B)**. In animal model, we determined that 10 μM, 500 nM, and 100 nM FR180204 did not induce significant alterations in retinal thickness and RPE morphology when analyzed by H&E staining (Fig. 6A). However, in 10 μM, but not in 100 nM FR180204-administered mouse, HRF were detected in the retina by SD-OCT (Fig. 6B). Given that the retina has multiple layers containing various types of cells, including ganglion cells, bipolar cells, horizontal cells, amacrine cells, and photoreceptors, in addition to the RPE cells located at the border of the retina, we decided to treat with 10 μM FR180204 in ARPE-19 cells and 100 nM FR180204 in mouse eyes to attenuate the activation of ERK by $NaIO_3$.

In the treatment of AMD, anti-VEGF is the most common therapy for wet AMD [26,27], however, there are currently no effective treatments for the most common form, dry AMD [28,70]. $NaIO_3$-induced retinal degeneration is widely used to study dry AMD [19]. To investigate the potential therapeutic applicability of FR180204, we applied the mouse model to test its effects *in vivo*. Consistent with the results of previous studies [15], we observed the characteristic phenotype with the degenerative RPE layer showing disintegration and initiation of translocation after the treatment with $NaIO_3$ (Fig. 1**F and 7B**). In addition, we identified that the structural changes of the retina induced by $NaIO_3$ were restored by FR180204 analyzed by immunofluorescence and histological analysis (Figs. 6 and 7). We applied SD-OCT and identified a pattern of HRF (Fig. 8), whose clinicopathological significance has been widely investigated [71], indicative of the migration of RPE cells, macrophages/microglia in AMD [79–81], and lipoprotein extravasation in diabetic macular edema [82].

Conclusion

Intracellular ROS, Ca^{2+}, ER stress marker, p-ERK, p-EGFR, and EMT markers were enhanced in $NaIO_3$-stimulated cells. Most importantly, ERK activation was found to play a critical role in regulating the progression of various $NaIO_3$-induced pathways leading to EMT in RPE cells. The attenuation of ERK activation, multiple $NaIO_3$-induced signaling pathways, and EMT in RPE cells by post-treatment with FR180204, an ERK inhibitor and potential cancer drug, may be a new therapeutic approach for AMD.

Ethics approval and consent to participate

All experimental procedures have been approved by the Institutional Review Committee at Taipei Veterans General Hospital.

Availability of data and materials

The datasets used and/or analyzed during the current study are available from the corresponding author on a reasonable request.

Declaration of Competing Interest

The authors declare that they have no known competing financial interests or personal relationships that could have appeared to influence the work reported in this paper.

Acknowledgement

This research was funded by the National Science and Technology Council (NSTC 111-2321-B-A49-009 and NSTC 112-2321-B-A49-007), and Taipei Veterans General Hospital (V111C-014, 111VACS-003, and 111VACS-007). This work was financially supported by the "Center for Intelligent Drug Systems and Smart Bio-devices (IDS2B) "from The Featured Areas Research Center Program within the framework of the Higher Education Sprout Project by the Ministry of Education (MOE) in Taiwan. This work was supported by the Center of Stem Cell in Taipei Veterans General Hospital. We thank Ming-Long Tsai, Chia-Lin Wang, Yu-Ling Ko, Hsiao-Yun Tai, Yi-Ching Tsai, Yun-Ju Fu, and Fu-Ting Tsai for providing valuable technical consultation.

Appendix A. Supplementary material

Supplementary data to this article can be found online at https://doi.org/10.1016/j.jare.2023.06.004.

References

[1] Reibaldi M, Longo A, Pulvirenti A, Avitabile T, Russo A, Cillino S, et al. Geo-epidemiology of age-related macular degeneration: new clues into the pathogenesis. Am J Ophthalmol 2016;161. doi: https://doi.org/10.1016/j.ajo.2015.09.031. 78–93.e1-2.

[2] Young RW. Pathophysiology of age-related macular degeneration. Surv Ophthalmol 1987;31:291–306. doi: https://doi.org/10.1016/0039-6257(87)90115-9.

[3] Datta S, Cano M, Ebrahimi K, Wang L, Handa JT. The impact of oxidative stress and inflammation on RPE degeneration in non-neovascular AMD. Prog Retin Eye Res 2017;60:201–18. doi: https://doi.org/10.1016/j.preteyeres.2017.03.002.

[4] Miceli MV, Liles MR, Newsome DA. Evaluation of oxidative processes in human pigment epithelial cells associated with retinal outer segment phagocytosis. Exp Cell Res 1994;214:242–9. doi: https://doi.org/10.1006/excr.1994.1254.

[5] Plafker SM, O'Mealey GB, Szweda LI. Mechanisms for countering oxidative stress and damage in retinal pigment epithelium. Int Rev Cell Mol Biol 2012;298:135–77. doi: https://doi.org/10.1016/B978-0-12-394309-5.00004-3.

[6] Ghosh S, Shang P, Terasaki H, Stepicheva N, Hose S, Yazdankhah M, et al. A role for βA3/A1-crystallin in type 2 EMT of RPE cells occurring in dry age-related macular degeneration. Invest Ophthalmol Vis Sci 2018;59:AMD104–13. 10.1167/iovs.18-24132.

[7] Kalluri R, Weinberg RA. The basics of epithelial-mesenchymal transition. J Clin Invest 2009;119:1420–8. doi: https://doi.org/10.1172/JCI39104.

[8] Zhou M, Geathers JS, Grillo SL, Weber SR, Wang W, Zhao Y, et al. Role of epithelial-mesenchymal transition in retinal pigment epithelium dysfunction. Front Cell Dev Biol 2020;8:501–13. doi: https://doi.org/10.3389/fcell.2020.00501.

[9] Tamiya S, Liu L, Kaplan HJ. Epithelial-mesenchymal transition and proliferation of retinal pigment epithelial cells initiated upon loss of cell-cell contact. Invest Ophthalmol Vis Sci 2010;51:2755–63. doi: https://doi.org/10.1167/iovs.09-4725.

[10] Flannery JG, Farber DB, Bird AC, Bok D. Degenerative changes in a retina affected with autosomal dominant retinitis pigmentosa. Invest Ophthalmol Vis Sci 1989;30:191–211.

[11] Li ZY, Possin DE, Milam AH. Histopathology of bone spicule pigmentation in retinitis pigmentosa. Ophthalmology 1995;102:805–16. doi: https://doi.org/10.1016/s0161-6420(95)30953-0.

[12] Morino I, Hiscott P, McKechnie N, Grierson I. Variation in epiretinal membrane components with clinical duration of the proliferative tissue. Br J Ophthalmol 1990;74:393–9. doi: https://doi.org/10.1136/bjo.74.7.393.

[13] Casaroli-Marano RP, Pagan R, Vilaró S. Epithelial-mesenchymal transition in proliferative vitreoretinopathy: intermediate filament protein expression in retinal pigment epithelial cells. Invest Ophthalmol Vis Sci 1999;40:2062–72.

[14] Hsu M-Y, Hsiao Y-P, Lin Y-T, Chen C, Lee C-M, Liao W-C, et al. Quercetin alleviates the accumulation of superoxide in sodium iodate-induced retinal autophagy by regulating mitochondrial reactive oxygen species homeostasis through enhanced deacetyl-SOD2 via the Nrf2-PGC-1α-Sirt1 pathway. Antioxidants (Basel) 2021;10:1125. doi: https://doi.org/10.3390/antiox10071125.

[15] Hanus J, Anderson C, Sarraf D, Ma J, Wang S. Retinal pigment epithelial cell necroptosis in response to sodium iodate. Cell Death Discovery 2016;2:1–9. doi: https://doi.org/10.1038/cddiscovery.2016.54.

[16] Chang Y-Y, Lee Y-J, Hsu M-Y, Wang M, Tsou S-C, Chen C-C, et al. Protective effect of quercetin on sodium iodate-induced retinal apoptosis through the reactive oxygen species-mediated mitochondrion-dependent pathway. Int J Mol Sci 2021;22:4056. doi: https://doi.org/10.3390/ijms22084056.

[17] Yang Y, Qin YJ, Yip YWY, Chan KP, Chu KO, Chu WK, et al. Green tea catechins are potent anti-oxidants that ameliorate sodium iodate-induced retinal degeneration in rats. Sci Rep 2016;6:29546. doi: https://doi.org/10.1038/srep29546.

[18] Chan C-M, Huang D-Y, Sekar P, Hsu S-H, Lin W-W. Reactive oxygen species-dependent mitochondrial dynamics and autophagy confer protective effects in retinal pigment epithelial cells against sodium iodate-induced cell death. J Biomed Sci 2019;26:40. doi: https://doi.org/10.1186/s12929-019-0531-z.

[19] Enzbrenner A, Zulliger R, Biber J, Pousa AMQ, Schäfer N, Stucki C, et al. Sodium iodate-induced degeneration results in local complement changes and inflammatory processes in murine retina. Int J Mol Sci 2021;22:9218. doi: https://doi.org/10.3390/ijms22179218.

[20] Kannan R, Hinton DR. Sodium iodate induced retinal degeneration: new insights from an old model. Neural Regen Res 2014;9:2044–5. doi: https://doi.org/10.4103/1673-5374.147927.

[21] Machalińska A, Lubiński W, Kłos P, Kawa M, Baumert B, Penkala K, et al. Sodium iodate selectively injuries the posterior pole of the retina in a dose-dependent manner: morphological and electrophysiological study. Neurochem Res 2010;35:1819–27. doi: https://doi.org/10.1007/s11064-010-0248-6.

[22] Tong Y, Wang S. Not all stressors are equal: mechanism of stressors on RPE cell degeneration. Front Cell Dev Biol 2020;8:. doi: https://doi.org/10.3389/fcell.2020.591067591067.

[23] Davis FM, Azimi I, Faville RA, Peters AA, Jalink K, Putney JW, et al. Induction of epithelial-mesenchymal transition (EMT) in breast cancer cells is calcium signal dependent. Oncogene 2014;33:2307–16. doi: https://doi.org/10.1038/onc.2013.187.

[24] Li L, Qi L, Liang Z, Song W, Liu Y, Wang Y, et al. Transforming growth factor-β1 induces EMT by the transactivation of epidermal growth factor signaling through HA/CD44 in lung and breast cancer cells. Int J Mol Med 2015;36:113–22. doi: https://doi.org/10.3892/ijmm.2015.2222.

[25] Olea-Flores M, Zuñiga-Eulogio MD, Mendoza-Catalán MA, Rodríguez-Ruiz HA, Castañeda-Saucedo E, Ortuño-Pineda C, et al. Extracellular-signal regulated kinase: a central molecule driving epithelial-mesenchymal transition in cancer. Int J Mol Sci 2019;20:2885. doi: https://doi.org/10.3390/ijms20122885.

[26] S.D. Solomon K. Lindsley S.S. Vedula M.G. Krzystolik B.S. Hawkins Anti-vascular endothelial growth factor for neovascular age-related macular degeneration Cochrane Database Syst Rev 2019;3:CD005139. 10.1002/14651858.CD005139.pub4.

[27] Khanna S, Komati R, Eichenbaum DA, Hariprasad I, Ciulla TA, Hariprasad SM. Current and upcoming anti-VEGF therapies and dosing strategies for the treatment of neovascular AMD: a comparative review. BMJ Open Ophthalmol 2019;4:e000398.

[28] Stahl A. The diagnosis and treatment of age-related macular degeneration. Dtsch Arztebl Int 2020;117:513–20. doi: https://doi.org/10.3238/arztebl.2020.0513.

[29] Yang I-H, Tsai Y-T, Chiu S-J, Liu L-T, Lee H-H, Hou M-F, et al. Involvement of STIM1 and Orai1 in EGF-mediated cell growth in retinal pigment epithelial cells. J Biomed Sci 2013;20:41. doi: https://doi.org/10.1186/1423-0127-20-41.

[30] Park GB, Kim D. Cigarette smoke-induced EGFR activation promotes epithelial mesenchymal migration of human retinal pigment epithelial cells through regulation of the FAK-mediated Syk/Src pathway. Mol Med Rep 2018;17:3563–74. doi: https://doi.org/10.3892/mmr.2017.8355.

[31] Catarino S, Bento CF, Brito A, Murteira E, Fernandes AF, Pereira P. Regulation of the expression of interleukin-8 induced by 25-hydroxycholesterol in retinal pigment epithelium cells. Acta Ophthalmol 2012;90:e255–63. doi: https://doi.org/10.1111/j.1755-3768.2011.02350.x.

[32] Xiao G-Y, Mohanakrishnan A, Schmid SL. Role for ERK1/2-dependent activation of FCHSD2 in cancer cell-selective regulation of clathrin-mediated endocytosis. Proc Natl Acad Sci 2018;115:E9570–9. doi: https://doi.org/10.1073/pnas.1810209115.

[33] Tien S-C, Lee H-H, Yang Y-C, Lin M-H, Chen Y-J, Chang Z-F. The Shp2-induced epithelial disorganization defect is reversed by HDAC6 inhibition independent of Cdc42. Nat Commun 2016;7:10420. doi: https://doi.org/10.1038/ncomms10420.

[34] Yang Y-C, Fann M-J, Chang W-H, Tai L-H, Jiang J-H, Kao L-S. Regulation of sodium-calcium exchanger activity by creatine kinase under energy-compromised conditions. J Biol Chem 2010;285:28275–85. doi: https://doi.org/10.1074/jbc.M110.141424.

[35] Islam R, Corraya RM, Pasovic L, Khan AZ, Aass HCD, Eidet JR, et al. The effects of prolonged storage on ARPE-19 cells stored at three different storage temperatures. Molecules 2020;25. doi: https://doi.org/10.3390/molecules25245809.

[36] Chen M, Rajapakse D, Fraczek M, Luo C, Forrester JV, Xu H. Retinal pigment epithelial cell multinucleation in the aging eye - a mechanism to repair damage and maintain homoeostasis. Aging Cell 2016;15:436–45. doi: https://doi.org/10.1111/acel.12447.

[37] Argun M, Tök L, Uğuz AC, Çelik Ö, Tök ÖY, Naziroğlu M. Melatonin and amfenac modulate calcium entry, apoptosis, and oxidative stress in ARPE-19 cell culture exposed to blue light irradiation (405 nm). Eye (Lond) 2014;28:752–60. doi: https://doi.org/10.1038/eye.2014.50.

[38] N L, J I, T D, N W, A H, D A, et al. Iron chelation protects the retinal pigment epithelial cell line ARPE-19 against cell death triggered by diverse stimuli Invest Ophthalmol Vis Sci 50 2009 1440 1447 10.1167/iovs.08-2545.

[39] Chen J, Li L, Zhou Y, Zhang J, Chen L. Gambogic acid ameliorates high glucose–and palmitic acid–induced inflammatory response in ARPE-19 cells via activating Nrf2 signaling pathway: ex vivo. Cell Stress Chaperones 2021;26:367–75. doi: https://doi.org/10.1007/s12192-020-01182-1.

[40] Bhattarai N, Piippo N, Ranta-aho S, Mysore Y, Kaarniranta K, Kauppinen A. Effects of resvega on inflammasome activation in conjunction with dysfunctional intracellular clearance in retinal pigment epithelial (RPE) cells. Antioxidants (Basel) 2021;10:67. doi: https://doi.org/10.3390/antiox10010067.

[41] Yardeni T, Eckhaus M, Morris HD, Huizing M, Hoogstraten-Miller S. Retro-orbital injections in mice Lab Anim (NY) 2011;40:155–60. doi: https://doi.org/10.1038/laban0511-155.

[42] Chowers G, Cohen M, Marks-Ohana D, Stika S, Eijzenberg A, Banin E, et al. Course of sodium iodate–induced retinal degeneration in albino and pigmented mice. Invest Ophthalmol Vis Sci 2017;58:2239–49. doi: https://doi.org/10.1167/iovs.16-21255.

[43] Tsai H-Y, Lai HIAM, Chen Z-Y, Lin T-C, Khor W, Kuo W-C, et al. Inhibition of DUSP6 activates autophagy and rescues the retinal pigment epithelium in sodium iodate-induced retinal degeneration models in vivo and in vitro. Biomedicines 2022;10:159. doi: https://doi.org/10.3390/biomedicines10010159.

[44] Syu J-P, Buddhakosai W, Chen S-J, Ke C-C, Chiou S-H, Kuo W-C. Supercontinuum source-based multi-contrast optical coherence tomography for rat retina imaging. Biomed Opt Express 2018;9:6132. doi: https://doi.org/10.1364/BOE.9.006132.

[45] Zhang P, Zam A, Jian Y, Wang X, Li Y, Lam KS, et al. *In vivo* wide-field multispectral scanning laser ophthalmoscopy-optical coherence tomography mouse retinal imager: Longitudinal imaging of ganglion cells, microglia, and

Müller glia, and mapping of the mouse retinal and choroidal vasculature. J Biomed Opt 2015;20:. doi: https://doi.org/10.1117/1.JBO.20.12.126005126005.
[46] Tsai P-H, Chien Y, Wang M-L, Hsu C-H, Laurent B, Chou S-J, et al. Ash2l interacts with Oct4-stemness circuitry to promote super-enhancer-driven pluripotency network. Nucleic Acids Res 2019;47:10115–33. doi: https://doi.org/10.1093/nar/gkz801.
[47] Kawano H, Ito T, Yamada S, Hashiguchi T, Maruyama I, Hisatomi T, et al. Toxic effects of extracellular histones and their neutralization by vitreous in retinal detachment. Lab Invest 2014;94:569–85. doi: https://doi.org/10.1038/labinvest.2014.46.
[48] Toda T, Hsu JY, Linker SB, Hu L, Schafer ST, Mertens J, et al. Nup153 interacts with Sox2 to enable bimodal gene regulation and maintenance of neural progenitor cells. Cell Stem Cell 2017;21:618–634.e7. doi: https://doi.org/10.1016/j.stem.2017.08.012.
[49] Madreiter-Sokolowski CT, Thomas C, Ristow M. Interrelation between ROS and Ca^{2+} in aging and age-related diseases. Redox Biol 2020;36:. doi: https://doi.org/10.1016/j.redox.2020.101678101678.
[50] Zheng Y, Shen X. H_2O_2 directly activates inositol 1,4,5-trisphosphate receptors in endothelial cells. Redox Rep 2005;10:29–36. doi: https://doi.org/10.1179/135100005X21660.
[51] Loboda A, Damulewicz M, Pyza E, Jozkowicz A, Dulak J. Role of Nrf2/HO-1 system in development, oxidative stress response and diseases: an evolutionarily conserved mechanism. Cell Mol Life Sci 2016;73:3221. doi: https://doi.org/10.1007/s00018-016-2223-0.
[52] Görlach A, Bertram K, Hudecova S, Krizanova O. Calcium and ROS: A mutual interplay. Redox Biol 2015;6:260–71. doi: https://doi.org/10.1016/j.redox.2015.08.010.
[53] He H, Kuriyan AE, Su C-W, Mahabole M, Zhang Y, Zhu Y-T, et al. Inhibition of proliferation and epithelial mesenchymal transition in retinal pigment epithelial cells by heavy chain-hyaluronan/pentraxin 3. Sci Rep 2017;7:43736. doi: https://doi.org/10.1038/srep43736.
[54] Gonzalez DM, Medici D. Signaling mechanisms of the epithelial-mesenchymal transition. Sci Signal 2014;7:re8. 10.1126/scisignal.2005189.
[55] Čáslavský J, Klímová Z, Vomastek T. ERK and RSK regulate distinct steps of a cellular program that induces transition from multicellular epithelium to single cell phenotype. Cell Signal 2013;25:2743–51. doi: https://doi.org/10.1016/j.cellsig.2013.08.024.
[56] West SK, Rosenthal FS, Bressler NM, Bressler SB, Munoz B, Fine SL, et al. Exposure to sunlight and other risk factors for age-related macular degeneration. Arch Ophthalmol 1989;107:875–9. doi: https://doi.org/10.1001/archopht.1989.01070010897038.
[57] Delcourt C, Cougnard-Grégoire A, Boniol M, Carrière I, Doré J-F, Delyfer M-N, et al. Lifetime exposure to ambient ultraviolet radiation and the risk for cataract extraction and age-related macular degeneration: the alienor study. Invest Ophthalmol Vis Sci 2014;55:7619–27. doi: https://doi.org/10.1167/iovs.14-14471.
[58] Cano M, Thimmalappula R, Fujihara M, Nagai N, Sporn M, Wang AL, et al. Cigarette smoking, oxidative stress, the anti-oxidant response through Nrf2 signaling, and age-related macular degeneration. Vision Res 2010;50:652–64. doi: https://doi.org/10.1016/j.visres.2009.08.018.
[59] Bluteau J, Zulliger R, Roberti S, Enzmann V. Retinal cell death caused by sodium iodate involves multiple caspase-dependent and caspase-independent cell-death pathways. Int J Mol Sci 2015;16:15086–103. doi: https://doi.org/10.3390/ijms160715086.
[60] Safaei A, Brockmann J, Dick HB, Joachim SC. Apoptotic effects on human RPE cells through $NaIO_3$. Invest Ophthalmol Vis Sci 2022;63:773–F0332.
[61] Su Y, Tang Z, Wang F. Role of LINC01592 in TGF-β1-induced epithelial-mesenchymal transition of retinal pigment epithelial cells. Aging 2021;13(14053–64). doi: https://doi.org/10.18632/aging.203023.
[62] Cannito S, Novo E, di Bonzo LV, Busletta C, Colombatto S, Parola M. Epithelial-mesenchymal transition: from molecular mechanisms, redox regulation to implications in human health and disease. Antioxid Redox Signal 2010;12:1383–430. doi: https://doi.org/10.1089/ars.2009.2737.
[63] Cichon MA, Radisky DC. ROS-induced epithelial-mesenchymal transition in mammary epithelial cells is mediated by NF-κB-dependent activation of Snail. Oncotarget 2014;5(2827–38). doi: https://doi.org/10.18632/oncotarget.1940.
[64] Gibson GE, Zhang H, Xu H, Park LCH, Jeitner TM. Oxidative stress increases internal calcium stores and reduces a key mitochondrial enzyme. Biochim Biophys Acta (BBA) - Mol Basis Dis 2002;1586:177–89. doi: https://doi.org/10.1016/S0925-4439(01)00091-6.
[65] Yan Y, Wei C, Zhang W, Cheng H, Liu J. Cross-talk between calcium and reactive oxygen species signaling. Acta Pharmacol Sin 2006;27:821–6. doi: https://doi.org/10.1111/j.1745-7254.2006.00390.x.
[66] Dridi S, Hirano Y, Tarallo V, Kim Y, Fowler BJ, Ambati BK, et al. ERK1/2 activation is a therapeutic target in age-related macular degeneration. Proceedings of the National Academy of Sciences 2012;109:13781–6. 10.1073/pnas.1206494109.
[67] Zeng S, Zhang T, Chen Y, Chu-Tan J, Jin K, Lee S-R, et al. Inhibiting the activation of MAPK (ERK1/2) in stressed Müller cells prevents photoreceptor degeneration. Theranostics 2022;12:6705–22. doi: https://doi.org/10.7150/thno.71038.
[68] Donovan M, Doonan F, Cotter TG. Differential roles of ERK1/2 and JNK in retinal development and degeneration. J Neurochem 2011;116:33–42. doi: https://doi.org/10.1111/j.1471-4159.2010.07056.x.
[69] Pyakurel A, Balmer D, Saba-El-Leil MK, Kizilyaprak C, Daraspe J, Humbel BM, et al. Loss of extracellular signal-regulated kinase 1/2 in the retinal pigment epithelium leads to RPE65 decrease and retinal degeneration. Mol Cell Biol 2017;37:e00295–e317. doi: https://doi.org/10.1128/MCB.00295-17.
[70] de Guimaraes TAC, Varela MD, Georgiou M, Michaelides M. Treatments for dry age-related macular degeneration: therapeutic avenues, clinical trials and future directions. Br J Ophthalmol 2022;106:297–304. doi: https://doi.org/10.1136/bjophthalmol-2020-318452.
[71] Fragiotta S, Abdolrahimzadeh S, Dolz-Marco R, Sakurada Y, Gal-Or O, Scuderi G. Significance of hyperreflective foci as an optical coherence tomography biomarker in retinal diseases: characterization and clinical implications. J Ophthalmol 2021;2021:e6096017.
[72] Terluk MR, Ebeling MC, Fisher CR, Kapphahn RJ, Yuan C, Kartha RV, et al. N-Acetyl-L-cysteine protects human retinal pigment epithelial cells from oxidative damage: implications for age-related macular degeneration. Oxid Med Cell Longev 2019;2019:5174957. doi: https://doi.org/10.1155/2019/5174957.
[73] Qin S, Lu Y, Rodrigues GA. Resveratrol protects RPE cells from sodium iodate by modulating PPARα and PPARδ. Exp Eye Res 2014;118:100–8. doi: https://doi.org/10.1016/j.exer.2013.11.010.
[74] Zha X, Wu G, Zhao X, Zhou L, Zhang H, Li J, et al. PRDX6 protects ARPE-19 cells from oxidative damage via PI3K/AKT signaling. CPB 2015;36:2217–28. doi: https://doi.org/10.1159/000430186.
[75] Dvashi Z, Goldberg M, Adir O, Shapira M, Pollack A. TGF-β1 induced transdifferentiation of RPE cells is mediated by TAK1. PLoS One 2015;10:e0122229.
[76] Ohori M, Takeuchi M, Maruki R, Nakajima H, Miyake H. FR180204, a novel and selective inhibitor of extracellular signal-regulated kinase, ameliorates collagen-induced arthritis in mice. Naunyn Schmiedebergs Arch Pharmacol 2007;374:311–6. doi: https://doi.org/10.1007/s00210-006-0117-7.
[77] Dirican A, Atmaca H, Bozkurt E, Erten C, Karaca B, Uslu R. Novel combination of docetaxel and thymoquinone induces synergistic cytotoxicity and apoptosis in DU-145 human prostate cancer cells by modulating PI3K–AKT pathway. Clin Transl Oncol 2014;17:145–51. doi: https://doi.org/10.1007/s12094-014-1206-6.
[78] Saglam ASY, Alp E, Elmazoglu Z, Menevse ES. Effect of API-1 and FR180204 on cell proliferation and apoptosis in human DLD-1 and LoVo colorectal cancer cells. Oncol Lett 2016;12:2463–74. doi: https://doi.org/10.3892/ol.2016.4995.
[79] Framme C, Wolf S, Wolf-Schnurrbusch U. Small dense particles in the retina observable by spectral-domain optical coherence tomography in age-related macular degeneration. Invest Ophthalmol Vis Sci 2010;51:5965–9. doi: https://doi.org/10.1167/iovs.10-5779.
[80] Pang CE, Messinger JD, Zanzottera EC, Freund KB, Curcio CA. The onion sign in neovascular age-related macular degeneration represents cholesterol crystals. Ophthalmology 2015;122:2316–26. doi: https://doi.org/10.1016/j.ophtha.2015.07.008.
[81] C.A. Curcio E.C. Zanzottera T. Ach C. Balaratnasingam K.B. Freund Activated retinal pigment epithelium, an optical coherence tomography biomarker for progression in age-related macular degeneration Invest Ophthalmol Vis Sci 58 2017 BIO211 –26 10.1167/iovs.17-21872.
[82] Bolz M, Schmidt-Erfurth U, Deak G, Mylonas G, Kriechbaum K, Scholda C, et al. Optical coherence tomographic hyperreflective foci: a morphologic sign of lipid extravasation in diabetic macular edema. Ophthalmology 2009;116:914–20. doi: https://doi.org/10.1016/j.ophtha.2008.12.039.